S.P. Garbo

(1)

NASA Technical Memorandum 78783

AN EVALUATION OF THE SANDWICH BEAM IN FOUR-POINT BENDING AS A COMPRESSIVE TEST METHOD FOR COMPOSITES

Mark J. Shuart
Carl T. Herakovich

September 1978

NASA
National Aeronautics and Space Administration
Langley Research Center
Hampton, Virginia 23665

AN EVALUATION OF THE SANDWICH BEAM IN FOUR-POINT BENDING AS A COMPRESSIVE TEST METHOD FOR COMPOSITES

Mark J. Shuart

Langley Research Center

Hampton, Virginia

Carl T. Herakovich

Virginia Polytechnic Institute and State University

Blacksburg, Virginia

TABLE OF CONTENTS

LIST OF TABLES

LIST OF FIGURES

LIST OF SYMBOLS

$\bar{E}$	average Young's modulus
E	Young's modulus
F	nodal force
G	shear modulus
H	laminate half thickness
$[K]$	nodal stiffness matrix
M	inplane moment resultant
N	inplane force resultant
n	number of plys
$[Q]$	reduced stiffness matrix
$[\bar{Q}]$	transformed stiffness matrix
$[T]$	tensor transformation matrix
ΔT	temperature change
u	nodal displacement
z	distance from midplane of laminate
$\bar{\alpha}$	average coefficient of thermal expansion
α	coefficient of thermal expansion
γ°	midplane shear strain
γ	shear strain
ε°	midplane strain
ε	strain
θ	angle measured from x-axis
κ	midplane curvature
$\bar{\nu}$	average Poisson's ratio
ν	Poisson's ratio

σ	stress
$\bar{\sigma}$	average stress
τ	shear stress
$\bar{\tau}$	average shear stress

Superscripts

k	*ply number*
T	thermal
u	ultimate

Subscripts

Al	aluminum
k	ply number
ℓ	element number
m	mechanical
t	thermal
(L,W,T)	honeycomb coordinate system
(x,y,z)	laminate coordinate system
(1,2,3)	natural coordinate system

Chapter 1

INTRODUCTION

The need for high specific modulus and high specific strength materials has led to the development of fiber reinforced composite materials. Initially, glass fibers in a resin matrix were introduced, and they continue to be used in many applications. However, a more recent class of composites called "advanced composites" utilizes much higher modulus fibers (e.g. graphite fibers are four to nine times stiffer than glass fibers). These advanced composites have been successfully used in a variety of aerospace applications as replacements for stiffness critical components.

As with any material, the efficient use of composites depends on a sound understanding of the material behavior. This understanding is of particular importance to the designer whose success depends on reliable input data. Fundamental tests for material property characterization need to be performed to obtain these data. However, investigators often disagree on the most accurate test methods for obtaining design data. Compression testing is one area of material characterization for which many methods and specimen geometries have been proposed. Minimal documentation of the limitations of current compressive test methods has appeared in the literature. Hence, considerable testing and analysis must be accomplished before any test method can be universally accepted as the most accurate.

This study considers the acceptability of the honeycomb sandwich beam in four-point bending as a reliable compressive test method

for advanced composite materials. The evaluation of the test method is based on two criteria: (1) the existence of a uniform compressive stress state in the test section of the beam and (2) an assessment of specimen geometry effects on that stress state.

To accomplish this evaluation, a literature review of compressive test methods for composite materials was performed. A graphite/polyimide sandwich beam was analyzed using a three-dimensional finite element computer program to assess the behavior of the compressed test section. Experimental data from the sandwich beam including data from the constituents were also obtained. Data from the constituent tests were used for input into the analysis. Honeycomb core compression specimens were tested at room temperature, and graphite/polyimide tensile specimens were tested at room temperature, -157°C (-250°F), and 316°C (600°F). Sandwich beam compression specimens were tested at room temperature. Based on the analytical and experimental results conclusions were drawn as to the acceptability of the sandwich beam as a compressive test method.

Chapter 2

LITERATURE REVIEW

Many different test specimens have been used to obtain compressive data for composite materials. Some of these specimens are quite similar having only differences in overall dimensions. The following is a review of the literature on compressive test specimens for composite materials. For simplicity the specimens are grouped by geometry.

2.1 Coupon Specimens

Coupon specimens have been used because of their low cost and simplicity in testing. The dogbone coupon [1-10] has been approved by the ASTM [1] for use in the testing of rigid plastics (Figure 1). For lack of any other standardized specimen, the dogbone coupon was initially used for the testing of advanced composites. The reduced cross-sectional area in the specimen's gage length promotes failure in a region removed from grip influence. Compressive strength data for composites have been specifically obtained using this specimen [2,4]. A major disadvantage of the dogbone coupon has been the end-brooming that occurs during load application. This brooming can initiate failure of the specimen. Also, when reducing the cross-sectional area of the specimen, continuous fibers are cut. The effect of cut fibers on specimen strength has generally been ignored when reporting data.

The rectangular coupon [2,5,8,11-20] was introduced to avoid cutting fibers in the specimen. Compressive modulus data have been primarily obtained from this specimen [2]. At least a ten percent scatter has

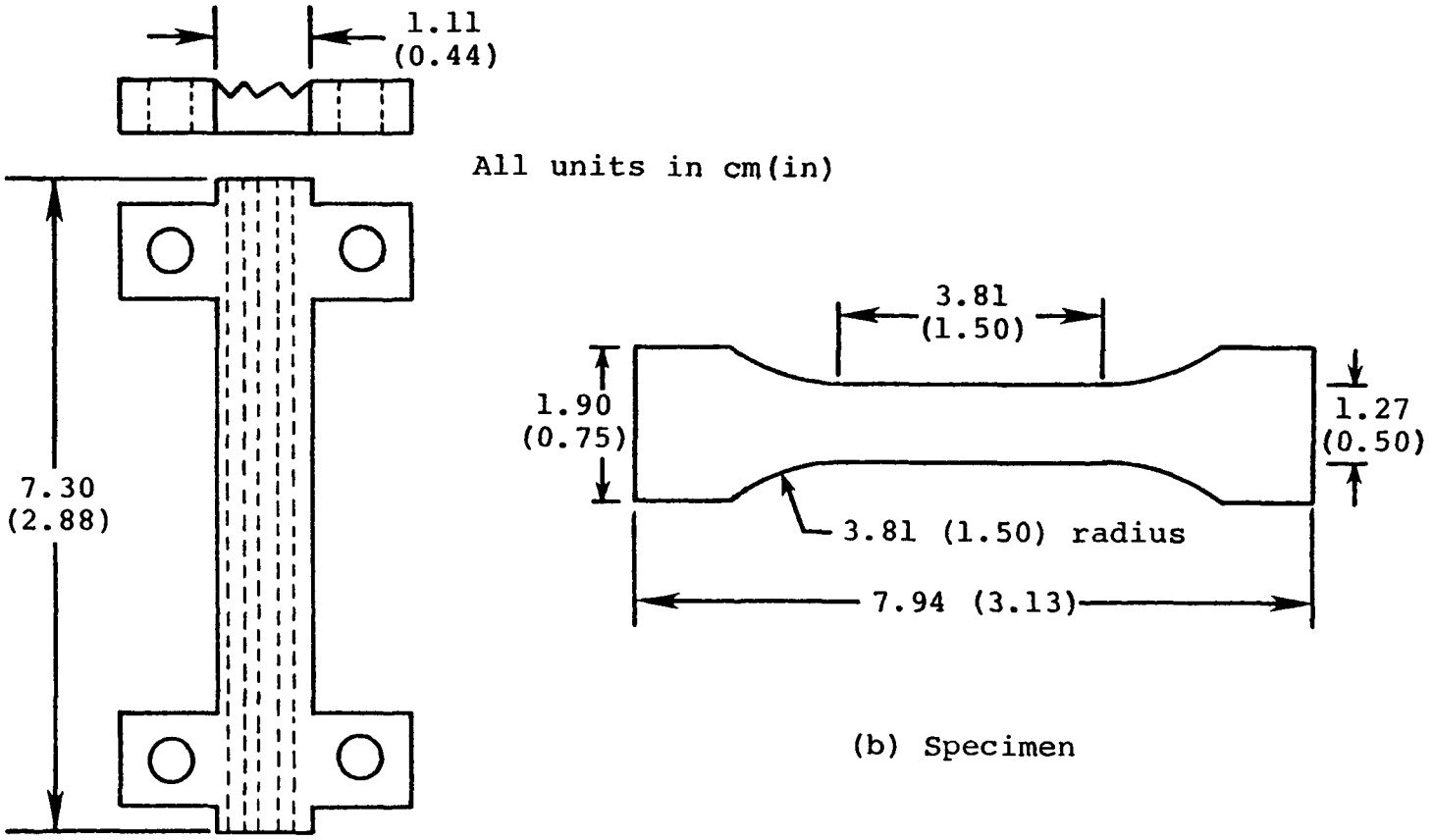

Figure 1. ASTM Dogbone Specimen with Reinforcing Fixture

been observed in the compressive strength data obtained from the rectangular coupon, but the degree of scatter was found to be a function of the specimen gage length [13,14]. The Celanese coupon used by Hofer et al [16] has become well known since being introduced in 1972. As shown in Figure 2, the specimen has a very short gage length when compared to the length of the tabbed region used for gripping. This coupon was used to obtain strength and modulus data. The ASTM [17] adopted a procedure that utilizes this specimen for the testing of oriented fiber composites. Ryder and Black [20] used a large gage length coupon for their study. Lateral and end supports were minimized during testing. Based on the results of two laminate configurations, the authors concluded that their procedure prevented end-brooming and buckling. Strength and modulus data were also reported in this study.

2.2 Tube Specimens

Tube specimens [6,8,15,21,22] have been used to obtain very acceptable compressive data. Typically, the ends of these specimens are potted to prevent end-brooming. However, difficulty in fabrication of the tubes has prevented wide-spread use of this specimen.

2.3 Cylindrical and Block Specimens

Solid cylindrical and block specimens have been used for testing unidirectional composites [6,8,13,14,18,23-25]. Other fiber orientations have not been tested with these specimens because of difficulties in fabrication. These specimens are typically compressed without grips or supports. The lack of restraint leads to some drawbacks. The

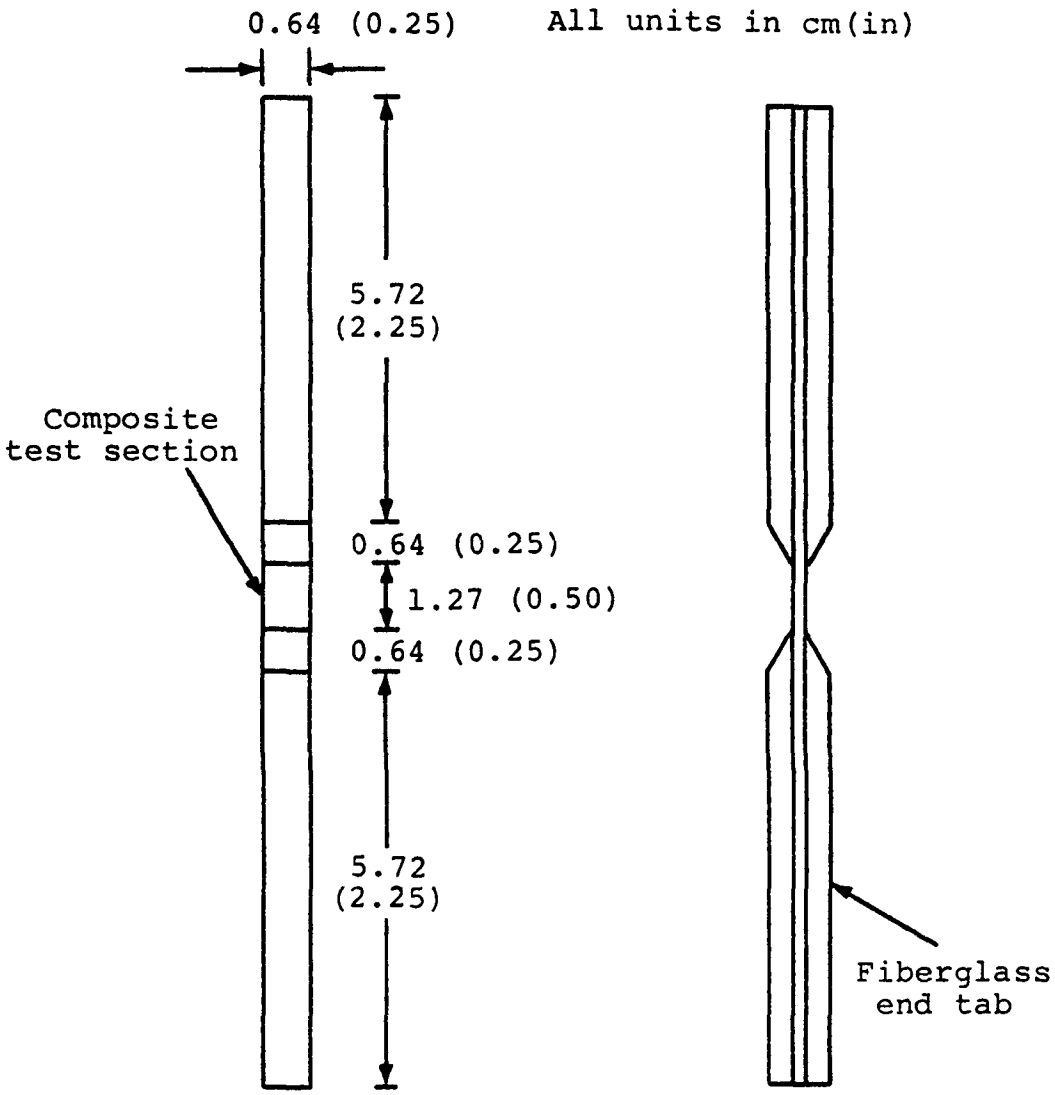

Figure 2. Celanese Compressive Coupon

unrestrained ends of the specimen have been observed to broom during the test thereby initiating failure [23-25]. This failure mode can be prevented by potting the ends in low modulus resin [13]. Weidner [24] reduced the cross-sectional area in the specimen's gage length to promote failure in this region. Although failures did occur in the gage length, the effect of the cut fibers again was not investigated.

2.4 Sandwich Specimens

Two types of sandwich specimens have been used for compressive testing. The edge-loaded compression specimen [9,16,26,27], as detailed by the ASTM [26], is shown in Figure 3. Face sheets are bonded to a honeycomb core which provides lateral stability to this specimen. The second type of sandwich specimen is the honeycomb sandwich beam shown in Figure 4 [8,11,13,16,27-29]. The specimen is loaded in four-point bending producing a constant moment in the center of the beam. This moment is statically equivalent to a couple which loads the composite flange in compression. Since the thickness of the composite flange is small compared to the height of the beam, it can be assumed that the compressive stress is constant through the composite thickness.

Some disadvantages exist for the sandwich specimens with cost being one of the most important. Compared to coupon specimens, large quantities of composite are required for the sandwich specimens. An observed disadvantage for the edge-loaded specimen has been the face wrinkling local instabilities [27] and end-brooming [16] which initiate failure. Local instabilities have also been observed for the

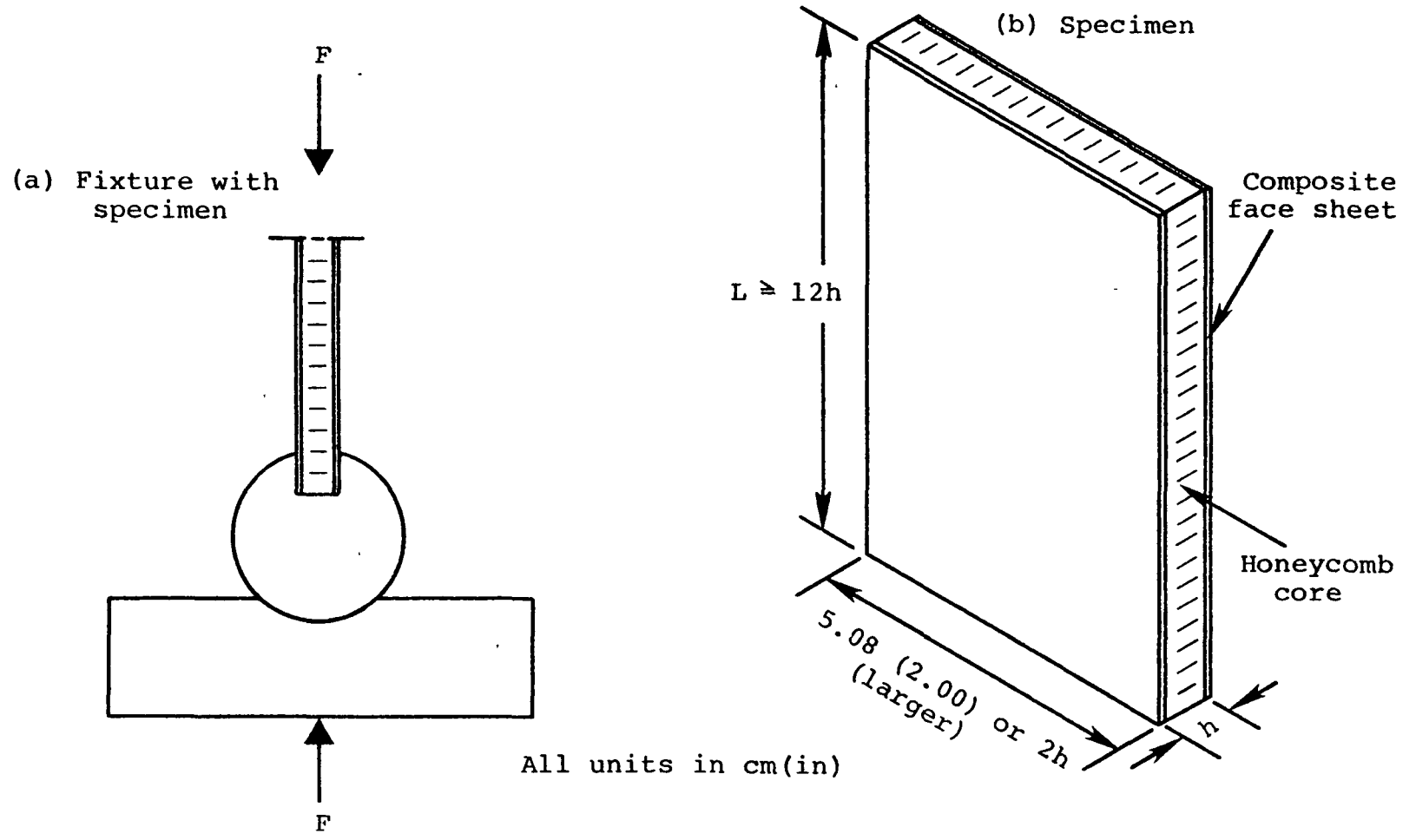

Figure 3. ASTM Edge-Loaded Fixture and Compressive Specimen

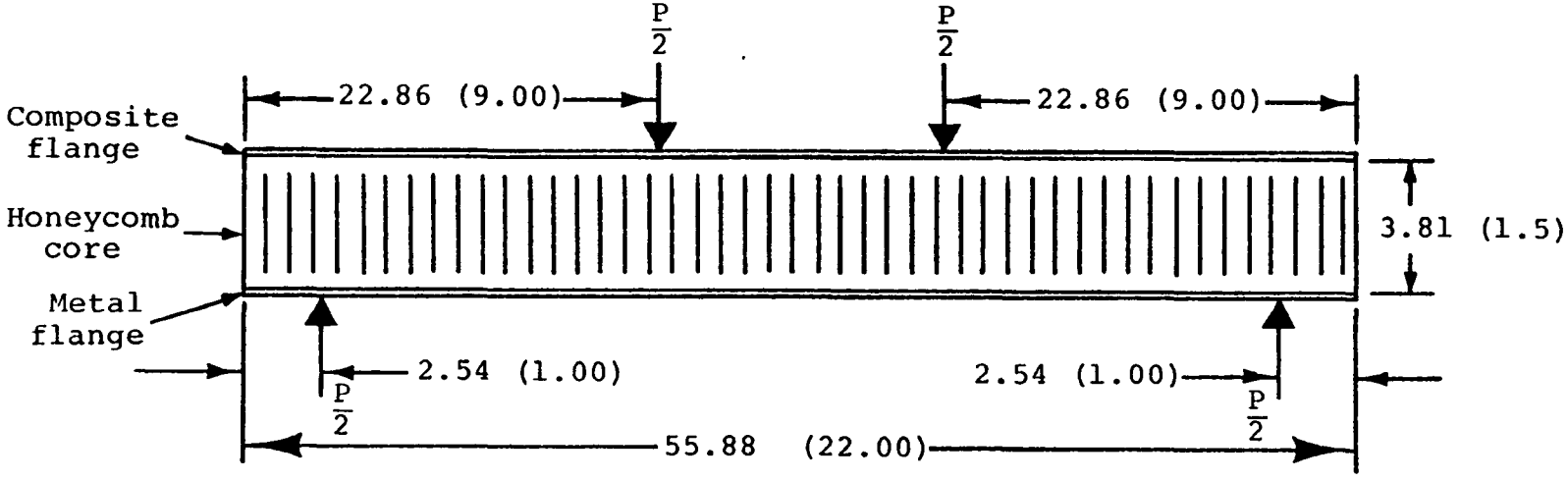

All units in cm(in)

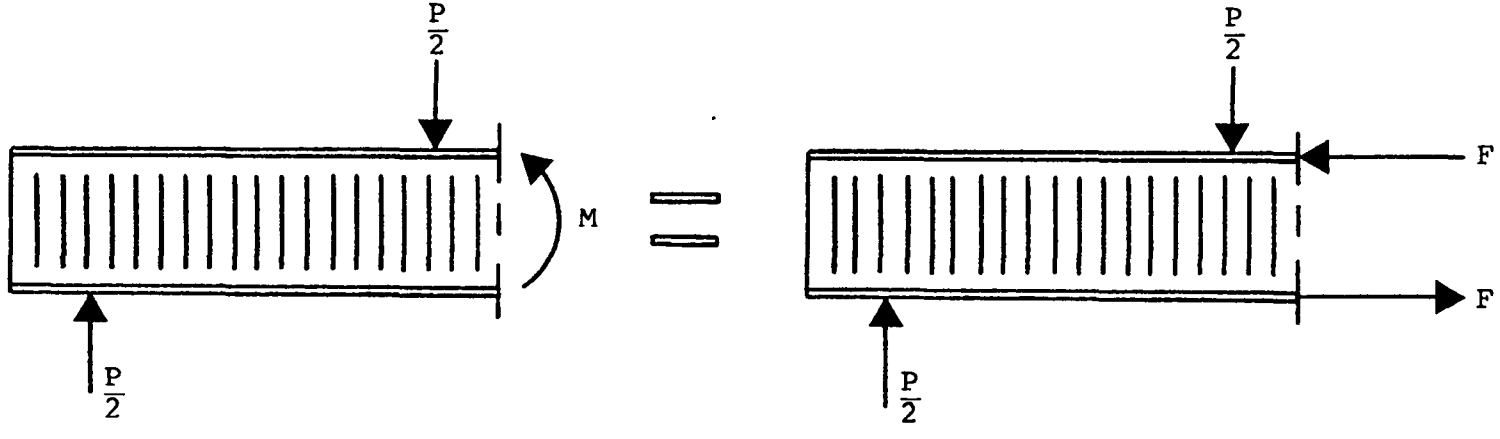

Figure 4. Sandwich Beam in Four-Point Bending

sandwich beam specimen [27]. Further, the beam is not easy to fabricate. The sandwich beam consists of a composite flange, a metal flange, and at most two types of honeycomb. The machining and bonding together of these components is a detailed if not difficult process.

2.5 Summary

Seven different specimen geometries for characterizing compressive behavior of advanced composites have been documented. Perhaps the most common criteria for evaluating these specimens have been cost and simplicity in testing. The coupon specimen is the first choice when specimens are evaluated by these criteria. Tube, cylindrical and block, and sandwich specimens are very costly when compared to coupons. However, an evaluation of all specimens based upon a detailed stress analysis does not appear to have been made. The influence of lateral restraints and specimen geometry have been neglected when analyzing data. Such a detailed stress analysis is necessary in order to properly evaluate generally the suitability of any particular geometry as a compression specimen. This investigation analyzes the honeycomb sandwich beam with particular attention to the influence of the honeycomb core on compressive test data.

Chapter 3

ANALYSIS

3.1 Laminate Equations

Laminate theory has been developed to predict orthotropic elastic material behavior. The fundamental element in the formulation is a lamina or single ply of material. The constitutive equations are developed for the orthotropic lamina and then extended to the laminate by simply adding the contributions from each ply. The theory also embodies the Kirchhoff plate assumptions which allow strains in any ply to be represented as a function of strains at the midplane and plate curvatures. A general formulation of the governing equations is outlined below; more specific details can be obtained from the literature [30-32].

Figure 5 shows lamina and laminate geometry with the two coordinate systems used in laminate theory. The most fundamental system is the natural (1,2) coordinate system shown in Figure 5a. This system is aligned with the natural material directions of a lamina (parallel and perpendicular to the fibers). However, the natural material directions of a ply may not always correspond to the principal geometric directions of a laminate. Hence, the laminate (x,y) coordinate system is introduced (Figure 5a). This system is convenient for laminate geometry where plies of different orientations are combined (Figure 5b).

A single ply of composite material is assumed to be homogeneous, orthotropic, and loaded in a state of plane stress. This leads to a

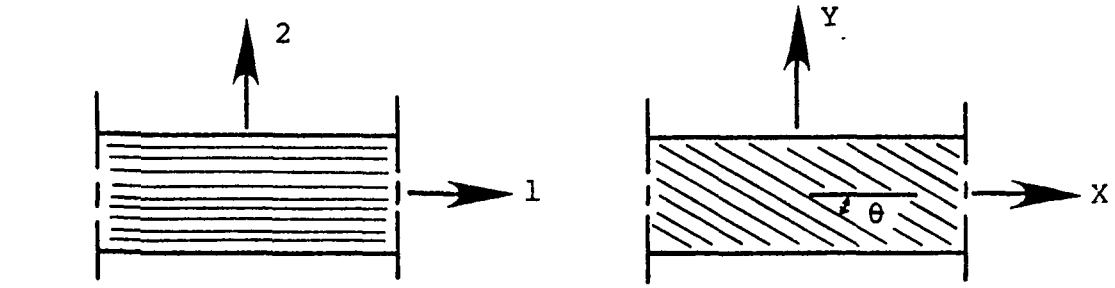

(a) Lamina

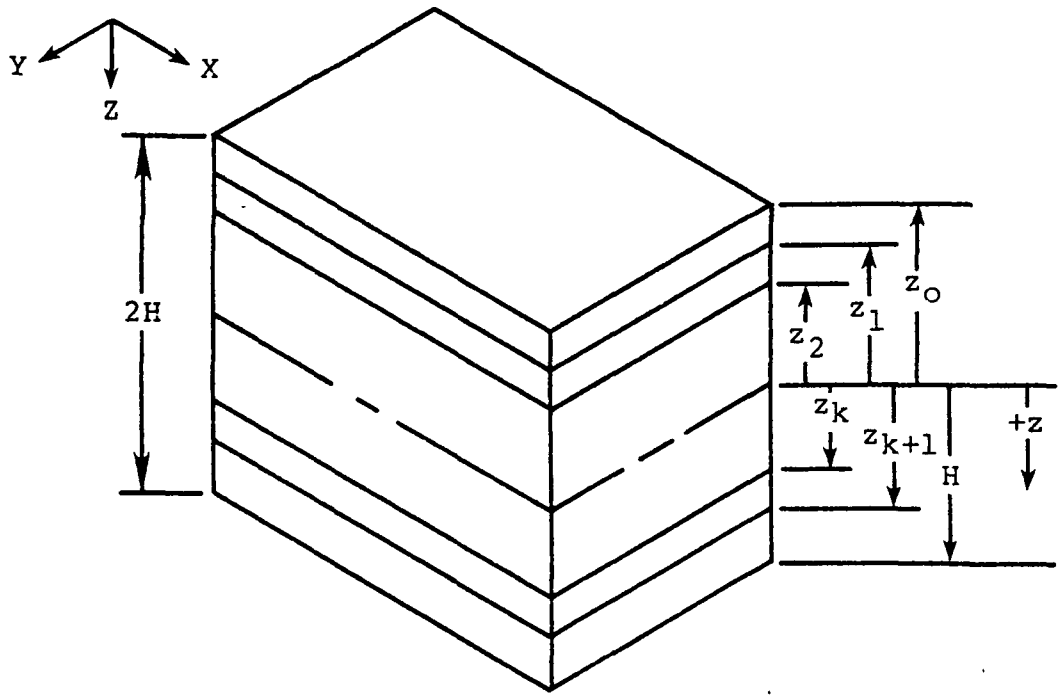

(b) Laminate

Figure 5. Lamina and Laminate Geometry

stress-strain relationship in the natural coordinate system of the form,

$$\begin{Bmatrix} \sigma_1 \\ \sigma_2 \\ \tau_{12} \end{Bmatrix} = \begin{bmatrix} Q_{11} & Q_{12} & 0 \\ Q_{12} & Q_{22} & 0 \\ 0 & 0 & Q_{66} \end{bmatrix} \begin{Bmatrix} \varepsilon_1 \\ \varepsilon_2 \\ \gamma_{12} \end{Bmatrix} \tag{3.1}$$

where the reduced stiffness matrix, [Q], is calculated from elastic engineering constants. An important relationship from Equ. (3.1) is,

$$\frac{\nu_{12}}{E_1} = \frac{\nu_{21}}{E_2} \tag{3.2}$$

This equation results from the symmetry of the material (reciprocal relation) [32]. Also, Equ. (3.1) can be expressed in the laminate coordinate system as,

$$\begin{Bmatrix} \sigma_x \\ \sigma_y \\ \tau_{xy} \end{Bmatrix} = \begin{bmatrix} \bar{Q}_{11} & \bar{Q}_{12} & \bar{Q}_{16} \\ \bar{Q}_{12} & \bar{Q}_{22} & \bar{Q}_{26} \\ \bar{Q}_{16} & \bar{Q}_{26} & \bar{Q}_{66} \end{bmatrix} \begin{Bmatrix} \varepsilon_x \\ \varepsilon_y \\ \gamma_{xy} \end{Bmatrix} \tag{3.3}$$

where the transformed stiffness matrix, $[\bar{Q}]$, is calculated from the reduced stiffness matrix, and transformation matrices, $[T_1]$ and $[T_2]$, i.e.

$$[\bar{Q}] = [T_1]^{-1}[Q][T_2] \tag{3.4}$$

where $[T_1]$ and $[T_2]$ are functions of the fiber angle θ.

A composite laminate behaves as the summation of its individual laminae. Hence, the laminate stress and moment stress resultants can

be calculated for a thickness of 2H,

$$\begin{Bmatrix} N_x \\ N_y \\ N_{xy} \end{Bmatrix} = \int_{-H}^{H} \begin{Bmatrix} \sigma_x \\ \sigma_y \\ \tau_{xy} \end{Bmatrix} dz \qquad \text{(a)}$$

$$\begin{Bmatrix} M_x \\ M_y \\ M_{xy} \end{Bmatrix} = \int_{-H}^{H} \begin{Bmatrix} \sigma_x \\ \sigma_y \\ \tau_{xy} \end{Bmatrix} z\,dz \qquad \text{(b)} \qquad (3.5)$$

where $\{\sigma\}$ is the stress at some point in the laminate and z is the distance from the midplane to that point (Figure 5b). Since the state of stress is assumed to be constant over each layer, Equ. (3.5) can be rewritten for an n-ply laminate,

$$\begin{Bmatrix} N_x \\ N_y \\ N_{xy} \end{Bmatrix} = \sum_{k=1}^{n} \int_{z_{k-1}}^{z_k} \begin{Bmatrix} \sigma_x \\ \sigma_y \\ \tau_{xy} \end{Bmatrix}^k dz \qquad \text{(a)}$$

$$\begin{Bmatrix} M_x \\ M_y \\ M_{xy} \end{Bmatrix} = \sum_{k=1}^{n} \int_{z_{k-1}}^{z_k} \begin{Bmatrix} \sigma_x \\ \sigma_y \\ \tau_{xy} \end{Bmatrix}^k z\,dz \qquad \text{(b)} \qquad (3.6)$$

where $\{\sigma\}^k$ is the stress state in the kth ply. Applying the Kirchhoff assumptions, the total strain in each ply can be written,

$$\begin{Bmatrix} \epsilon_x \\ \epsilon_y \\ \gamma_{xy} \end{Bmatrix} = \begin{Bmatrix} \epsilon_x^\circ \\ \epsilon_y^\circ \\ \gamma_{xy}^\circ \end{Bmatrix} + z \begin{Bmatrix} \kappa_x \\ \kappa_y \\ \kappa_{xy} \end{Bmatrix} \tag{3.7}$$

where $\{\epsilon^\circ\}$ are the midplane strains and $\{\kappa\}$ are the plate curvatures. Substituting Equ's. (3.3) and (3.7) into Equ. (3.6),

$$\{N\} = \sum_{k=1}^{n} \int_{z_{k-1}}^{z_k} [\bar{Q}]^k (\{\epsilon^\circ\} + z\{\kappa\}) dz \quad (a)$$

$$\{M\} = \sum_{k=1}^{n} \int_{z_{k-1}}^{z_k} [\bar{Q}]^k (\{\epsilon^\circ\} + z\{\kappa\}) z dz \quad (b) \tag{3.8}$$

Performing the indicated integrations, Equ. (3.8) becomes,

$$\{N\} = [A]\{\epsilon^\circ\} + [B]\{\kappa\} \quad (a)$$

$$\{M\} = [B]\{\epsilon^\circ\} + [D]\{\kappa\} \quad (b) \tag{3.9}$$

where by definition,

$$[A] = \sum_{k=1}^{n} [\bar{Q}]^k (z_k - z_{k-1}) \quad (a)$$

$$[B] = \frac{1}{2} \sum_{k=1}^{n} [\bar{Q}]^k (z_k^2 - z_{k-1}^2) \quad (b) \tag{3.10}$$

$$[D] = \frac{1}{3} \sum_{k=1}^{n} [\bar{Q}]^k (z_k^3 - z_{k-1}^3) \quad (c)$$

For the case of a symmetric laminate with no applied moment the governing equation can be expressed,

$$\{N\} = \begin{bmatrix} A_{11} & A_{12} & A_{16} \\ A_{12} & A_{22} & A_{26} \\ A_{16} & A_{26} & A_{66} \end{bmatrix} \{\varepsilon^\circ\} \tag{3.11}$$

Further, the average stress over the cross-section of the laminate, $\{\bar{\sigma}\}$, can be written,

$$\{\bar{\sigma}\} = \frac{1}{2H} \{N\} \tag{3.12}$$

Average elastic properties of the laminate for this case can be calculated from the basic definitions [33],

$$\bar{E}_x = \frac{\bar{\sigma}_x}{\varepsilon^\circ_x} \qquad \bar{\nu}_{xy} = -\frac{\varepsilon^\circ_y}{\varepsilon^\circ_x}$$

$$\bar{E}_y = \frac{\bar{\sigma}_y}{\varepsilon^\circ_y} \qquad \bar{\nu}_{yx} = -\frac{\varepsilon^\circ_x}{\varepsilon^\circ_y} \tag{3.13}$$

$$\bar{G}_{xy} = \frac{\bar{\tau}_{xy}}{\gamma^\circ_{xy}}$$

Applying Equ's. (3.11), (3.12), and (3.13) the average elastic properties can be expressed,

$$\bar{E}_x = \frac{1}{2Ha_{11}} \qquad \nu_{xy} = \frac{-a_{12}}{a_{11}}$$

$$\bar{E}_y = \frac{1}{2Ha_{22}} \qquad \nu_{yx} = \frac{-a_{12}}{a_{22}} \tag{3.14}$$

$$\bar{G}_{xy} = \frac{1}{2Ha_{66}}$$

where for simplicity,

$$\{a\} = [A]^{-1} \tag{3.15}$$

Using the average laminate properties, the axial midplane strain of the laminate can be expressed,

$$\varepsilon_x^o = \frac{1}{\bar{E}_x} (\bar{\sigma}_x - \bar{\nu}_{xy}\bar{\sigma}_y) \tag{3.16}$$

or factoring,

$$\varepsilon_x^o = \frac{\bar{\sigma}_x}{\bar{E}_x} (1 - \bar{\nu}_{xy} \frac{\bar{\sigma}_y}{\bar{\sigma}_x}) \tag{3.17}$$

Hence, the effect of a biaxial stress-state on the axial midplane strain is a function of the laminate Poisson's ratio and the ratio of average axial and transverse stresses.

Linear thermoelastic behavior can be easily incorporated into laminate theory. Assuming that the total strain in the laminate coordinate system of a lamina consists of mechanical and thermal components, the total strain can be written,

$$\{\varepsilon\}^k = \{\varepsilon\}_m^k + \{\varepsilon\}_t^k \tag{3.18}$$

The mechanical strain is obtained by inverting Equ. (3.3), and the thermal strain is calculated from,

$$\begin{Bmatrix} \varepsilon_x \\ \varepsilon_y \\ \gamma_{xy} \end{Bmatrix}^k_t = \begin{Bmatrix} \alpha_x \\ \alpha_y \\ \alpha_{xy} \end{Bmatrix}^k \Delta T \tag{3.19}$$

where $\{\alpha\}^k$ are the lamina coefficients of thermal expansion in the laminate coordinate system, and ΔT is the temperature change from the stress-free temperature. Combining Equ's. (3.3), (3.7), (3.18), and (3.19) the stress in the kth lamina can be written,

$$\{\sigma\}^k = [\bar{Q}]^k(\{\varepsilon^\circ\}+z\{\kappa\}-\{\alpha\}^k\Delta T) \tag{3.20}$$

Further, by using Equ's. (3.5), (3.6), (3.9), and (3.10) the stress and moment stress resultants can be expressed,

$$\begin{aligned} \{N\} &= [A]\{\varepsilon^\circ\}+[B]\{\kappa\}-\{N^T\} \qquad (a) \\ \{M\} &= [B]\{\varepsilon^\circ\}+[D]\{\kappa\}-\{M^T\} \qquad (b) \end{aligned} \tag{3.21}$$

where the equivalent thermal force and equivalent thermal moment, respectively, are defined,

$$\begin{aligned} \{N^T\} &= \int_{-H}^{H} [\bar{Q}]\{\alpha\}^k\Delta T dz \qquad (a) \\ \{M^T\} &= \int_{-H}^{H} [\bar{Q}]\{\alpha\}^k\Delta T z dz \qquad (b) \end{aligned} \tag{3.22}$$

The coefficient of thermal expansion for the laminate, $\{\bar{\alpha}\}$, can be

calculated by considering Equ. (3.21a) for the case of a symmetric laminate with a thermal stress resultant only, i.e.

$$\{N^T\} = [A]\{\varepsilon^\circ\} \tag{3.23}$$

For a uniform temperature distribution the coefficient will be related to the midplane strain,

$$\{\varepsilon^\circ\} = \{\bar{\alpha}\}\Delta T \tag{3.24}$$

which leads to the definition for temperature independent material properties,

$$\{\bar{\alpha}\} = [a] \int_{-H}^{H} [\bar{Q}]^k \{\alpha\}^k \, dz \tag{3.25}$$

3.2 Finite Element Model

The sandwich beam loaded in four-point bending produces a complex stress state in the test section of the specimen. This complex state of stress is a result of the variation of material properties within the beam. To examine the stress state in the test section of the beam, a three-dimensional finite element analysis was chosen. This approach considers the structure to be composed of many small, discrete elements. A portion of the beam's test section has been modeled using finite elements (Figure 6). This model leads to a better understanding of the stress state throughout the beam and, in particular, the composite flange.

The finite element approach considers element nodal displacements and element nodal forces. A variational principal, such as the mini-

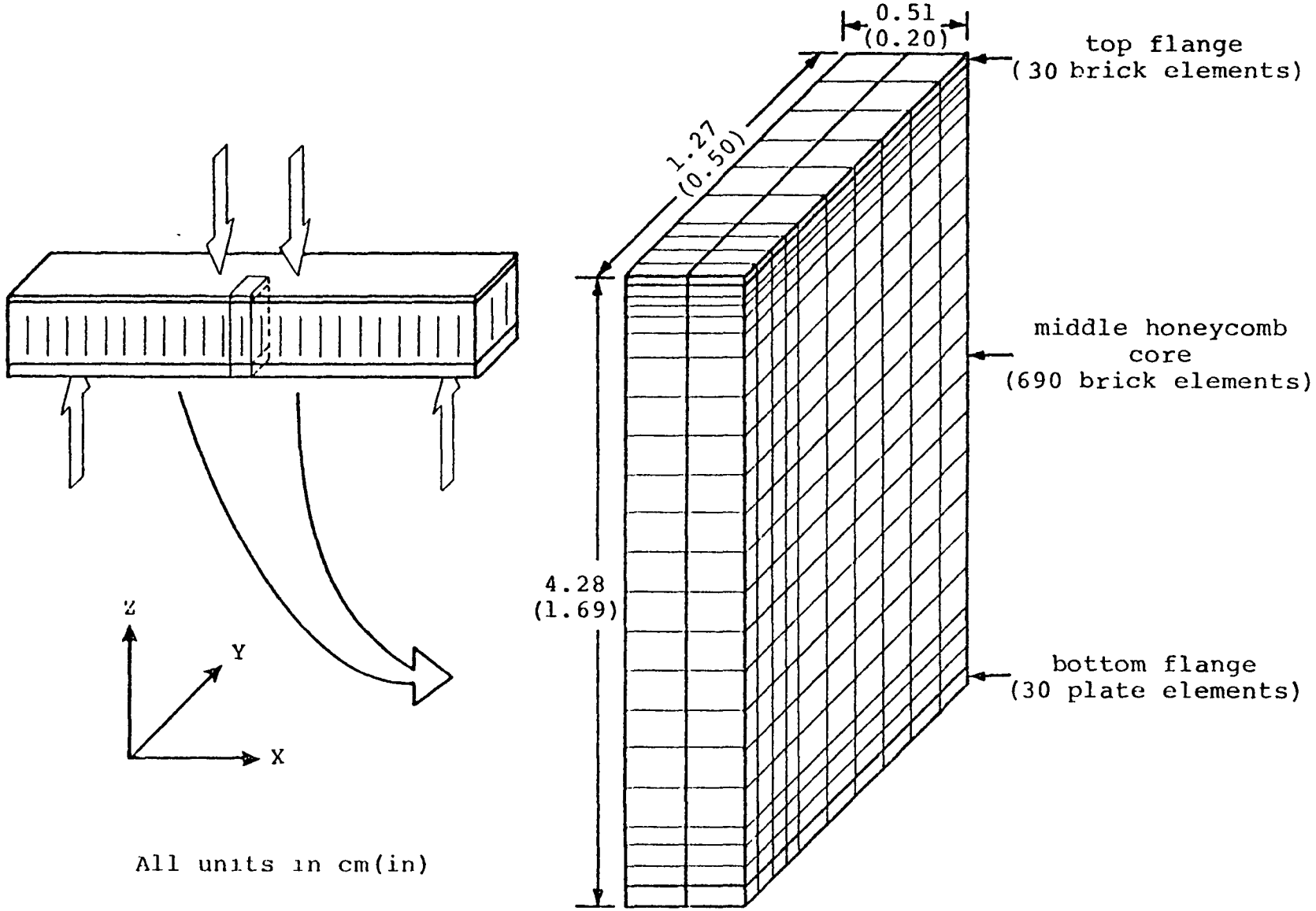

Figure 6. Schematic of Finite Element Model for Sandwich Beam

mization of potential energy, relates nodal forces $\{F\}_\ell$, to nodal displacements, $\{u\}_\ell$, through a stiffness matrix, $[K]_\ell$, and the relationship is written for the ℓth element as,

$$\{F\}_\ell = [K]_\ell\{u\}_\ell. \tag{3.26}$$

Equation (3.26) is written for each element in the model, and these equations are combined to obtain an expression relating the nodal forces and displacements for the entire model. For a specified loading and set of displacement boundary conditions the system of equations for the entire model is solved for the unknown displacements. Element stresses and strains can then be calculated from the nodal displacements, the strain-displacement equations, and the material constitutive equation.

The finite element computer program used in this study assumes linear, elastic material behavior. The assumption is also made that the composite flange and honeycomb core are homogeneous, orthotropic materials. The composite-honeycomb interface will be of particular interest in this analysis. Any effects the honeycomb core may have on composite behavior will be related to the stresses in this region.

The model for the finite element analysis of the sandwich beam test section is shown in Figure 6. A total of 750 elements and 1248 nodes are used. This is a three-dimensional analysis with each node having three translational degrees of freedom, u, v, and w. The model approximates a 0.51 cm x 1.27 cm x 4.28 cm (0.20 in x 0.50 in x 1.69 in) region of the beam test section as shown in the figure. The model is symmetric about the x,z-plane. The bottom metal flange is represented

as plate elements with isotropic material behavior. The top flange and honeycomb core are modeled by brick elements with orthotropic material behavior. The composite flange is assumed to have approximately the same elastic properties in tension and compression. The same assumption is also made for the honeycomb core.

The loading and displacement boundary conditions for the finite element model are shown in Figure 7. The moment acting in the beam test section is represented by the indicated linear displacement, U_0, across the y,z-plane. The boundary conditions shown in the figure insure the required symmetry and eliminate rigid body motion. The y-displacement boundary conditions on the GHIJ plane are zero reflecting the symmetry of the model. The only z-displacement boundary conditions are zero and along the neutral axis of the model. The location of the neutral axis is calculated from elementary theory [33].

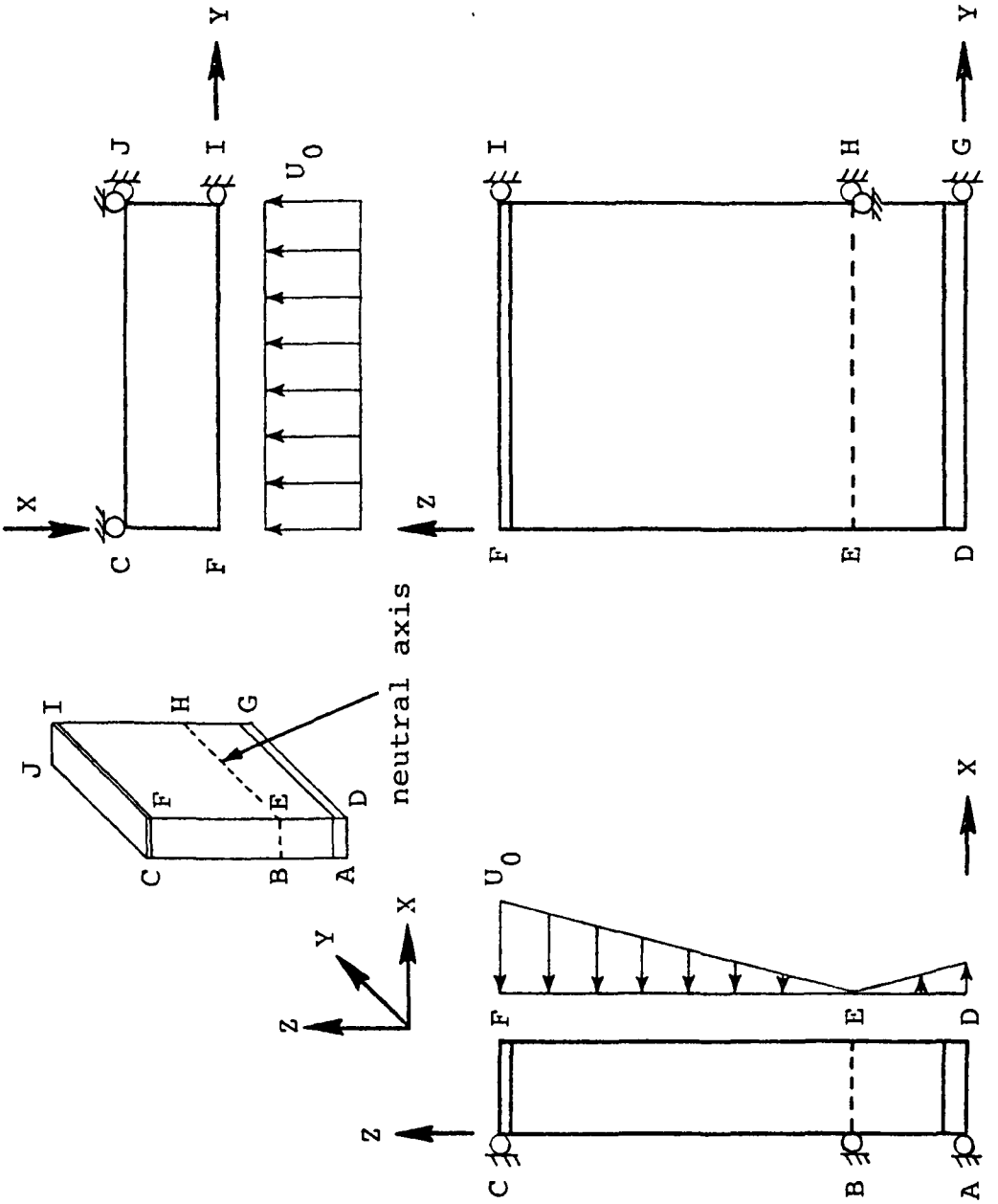

Figure 7. Loading and Displacement Boundry Conditions for Finite Element Model

Chapter 4

EXPERIMENTAL PROGRAM

The experimental program for this study was conducted in two phases. In the first phase, the individual constituents of the sandwich beam were tested to obtain data for analysis of the sandwich beam structure. Specifically, the aluminum honeycomb core in the beam test section was tested in compression at room temperature to obtain the Young's modulus and Poisson's ratio values not available in the literature, and graphite/polyimide tensile coupons were tested at -157°C (-250°F), room temperature, and 316°C (600°F) to obtain elastic material properties of the composite. The room temperature tensile results are used in the analysis of the sandwich beam test section since the composite is assumed to have approximately equal elastic properties in tension and compression. The second phase of the experimental program consisted of a series of room temperature compressive tests on both graphite/polymide laminates and 2024-T3 aluminum. The honeycomb sandwich beam specimen was used to obtain compressive ultimate stress, ultimate strain, Young's modulus, and Poisson's ratio values. Four different laminate orientations, $[0_8]$, $[90_8]$, $[(\pm 45)_2]_s$, and $[0/\pm 45/90]_s$, were tested during the course of the investigation. The specimens used for the tensile tests were machined from the same graphite/polyimide panels that supplied composite flanges for the sandwich beam specimens. The fiber volume fractions of the graphite/ polyimide panels ranged from fifty-three to fifty-five percent.

4.1 Test Specimens

Test specimens of beam constituents are shown in Figure 8. The honeycomb was 5052 aluminum, 0.318 cm (0.125 in) hexagonal cell size, 0.0038 cm (0.0015 in) wall thickness, 97.71 kg/m^3 (6.1 lb/ft^3) core density. The honeycomb compression specimens measured approximately 10.16 cm x 10.16 cm x 3.81 cm (4.00 in x 4.00 in x 1.50 in). The graphite/polyimide tensile specimens were fabricated from the HTS graphite fiber and the PMR-15 polyimide resin. Tensile specimens measured nominally 25.40 cm x 2.54 cm x 0.15 cm (10.00 in x 1.00 in x 0.06 in). Two glass/epoxy end tabs measuring 6.35 cm x 2.54 cm x 0.25 cm (2.50 in x 1.00 in x 0.10 in) were bonded to each end of the room temperature tensile specimens resulting in a 12.70 cm (5.00 in) test section. The tensile specimens tested at -157°C and 316°C had two glass/polyimide end tabs approximately 5.08 cm x 2.54 cm x 0.13 cm (2.00 in x 1.00 in x 0.05 in) bonded to each end of the specimens resulting in a 15.24 cm (6.00 in) test section. This tab material was used to minimize any thermal stresses that may be developed due to mismatch of thermal expansion between the tab and the specimen.

Figure 9 shows a honeycomb sandwich beam and its constituents. Nominal dimensions of beam specimens were 55.88 cm x 2.54 cm x 4.28 cm (22.00 in x 1.00 in x 1.68 in). Composite flanges approximately 0.15 cm (0.06 in) thick were fabricated from the HTS/PMR-15 graphite/polyimide system. Two different types of aluminum honeycomb core were used in the fabrication of some beams. The test section of the beam used the previously mentioned aluminum honeycomb. The other type of honeycomb

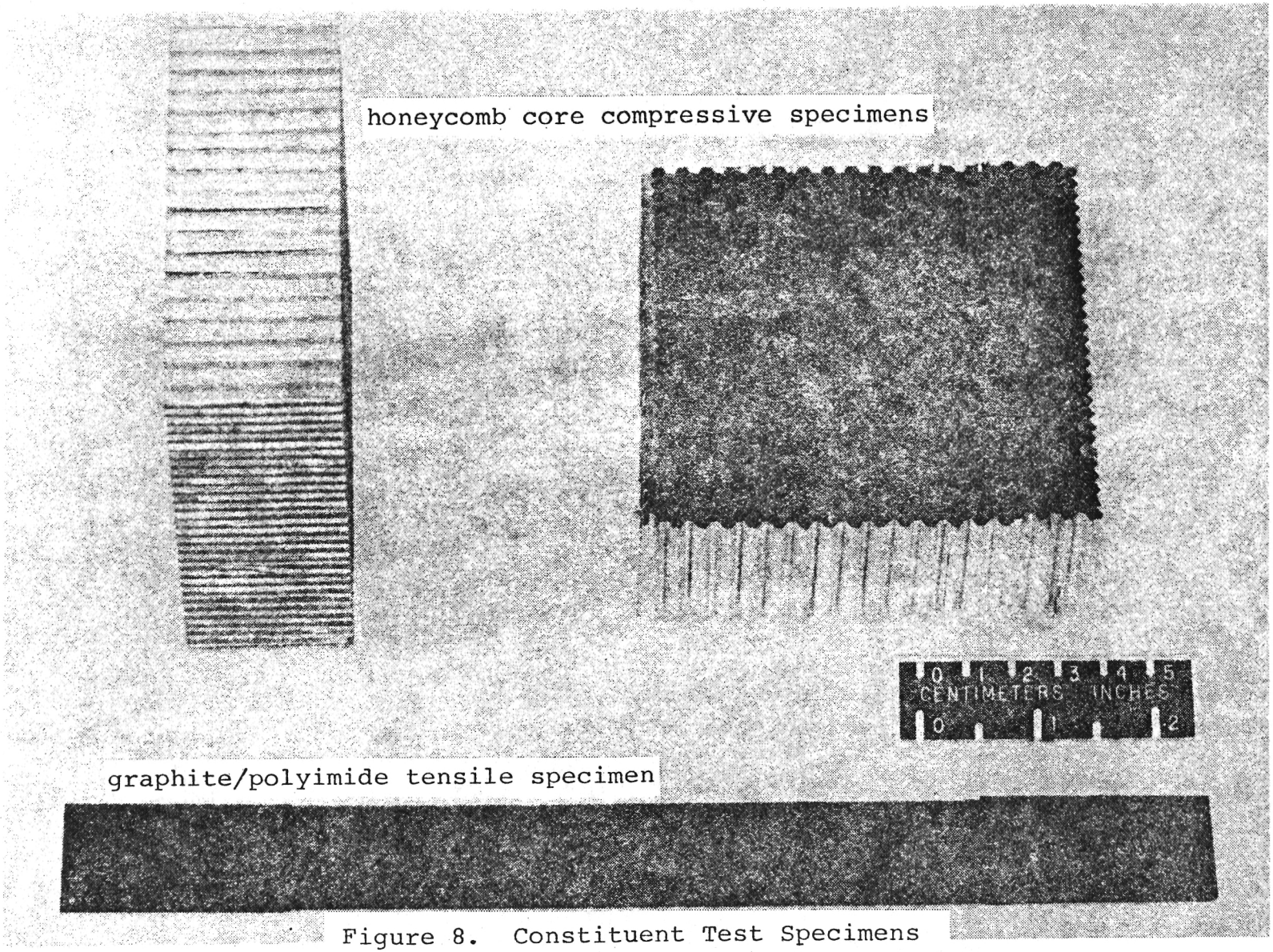

Figure 8. Constituent Test Specimens

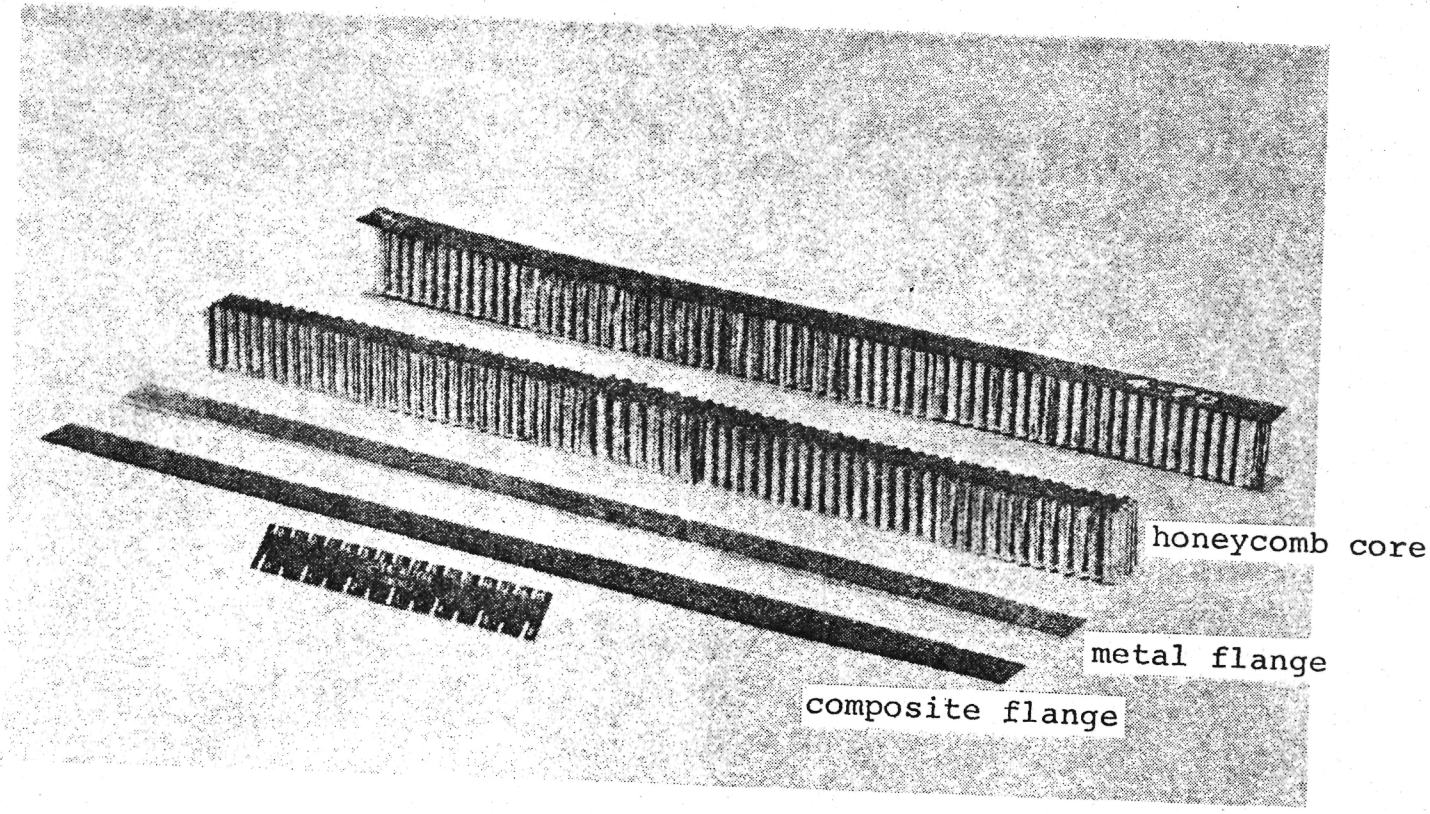

Figure 9. Sandwich Beam Specimen and Constituents

was 5052 aluminum, 0.318 cm (0.125 in) hexagonal cell size, 0.0152 cm (0.006 in) wall thickness, 254.0 kg/m^3 (22.1 lb/ft^3) core density. The denser honeycomb provides support at the points of load application and areas of transverse (through the beam thickness) shear load. A lighter honeycomb supports the beam test section. This region has no transverse shear load, and a lighter honeycomb is used to minimize any restraint on the composite test section. Beams having $[0_8]$, $[(\pm 45)_2]_s$, and $[0/\pm 45/90]_s$ composite flanges were fabricated using the two honeycomb cores. Beams having $[90_8]$ flanges were fabricated using only the lighter honeycomb core since the failure load for these specimens was lower than the other laminate orientations. The bottom flange of the beam specimen measured approximately 0.32 cm (0.12 in) in thickness and was either 2024-T3 aluminum or Ti-6Al-4V titanium. The bottom metal flange must be stronger than the top composite flange so that the top flange fails in compression prior to tensile failure of the bottom flange. Because the $[0_8]$ laminates exhibit failure loads significantly higher than the other laminates, a Ti-6Al-4V bottom flange was used for these beams. All other bottom flanges were 2024-T3.

The honeycomb sandwich beam specimens for obtaining 2024-T3 aluminum data were quite similar to the other beam specimens. The 2024-T3 beams measured approximately 55.88 cm x 2.54 cm x 4.44 cm (22.00 in x 1.00 in x 1.75 in), length, width, and height, respectively. These beams were fabricated using only the 97.71 kg/m^3 (6.1 lb/ft^3) aluminum honeycomb. The top and bottom flanges were 0.318 cm (0.125 in) thick 2024-T3.

4.2 Test Procedures

The 5052 aluminum honeycomb compressive specimens were tested in a 44,482 N (10,000 lbf) capacity Instron test machine. A constant strain rate was applied throughout the specimen's linear elastic range. Tests were terminated at the onset of material nonlinearity. Load and deflection data were obtained for determining Young's modulus and Poisson's ratio values. Deflection data were measured using linear variable differential transformers. The load and deflection data were plotted during the test on an x-y recorder. A total of four tests were performed.

The composite tensile specimens were tested in a 44,482 N (10,000 lbf) capacity Instron test machine, a 88,964 N (20,000 lbf) capacity Instron test machine or a 106,757 N (24,000 lbf) capacity Baldwin test machine. The capcity of the 44,482 N Instron machine was not sufficient for testing the $[0_8]$ specimens and, hence, the other machines were used to test these specimens. The Baldwin machine was used to test the $[0_8]$ specimens at room temperature and 316°C; the 88,964 N Instron machine was used to test the $[0_8]$ specimens at -157°C. For all tests at -157°C and 316°C each tensile specimen was enclosed in an insulated test chamber. The entire chamber was cooled or heated at a rate of approximately 7°C/min until the test temperature was reached. The test temperature was held for at least fifteen minutes prior to each test to ensure thermal equilibrium. Temperature was monitored before and during each test by a thermocouple adjacent to the test specimen. All tensile specimens were tested to failure. The Instron machines applied a

constant strain rate to failure; the Baldwin machine applied a constant load rate to failure. The strain rates were either 0.1 percent per minute or 0.2 percent per minute depending on the laminate tested, and the load rate was 13,345 N/min (3000 lbf/min). Load and strain data were obtained for determining Young's modulus and Poisson's ratio values. Strain data were measured using foil-type strain gages mounted on both sides of the tensile specimens. The $[0_8]$ and $[90_8]$ specimens had strain gages oriented at 0° and 90° with the load axis; the $[(\pm 45)_2]_s$ and $[0/\pm 45/90]_s$ specimens had strain rosettes oriented at 0°, 45°, and 90° with the load axis.* All data were recorded using an automatic multi-channel data acquisition system. Twenty-four tensile tests were performed: two tests for each of the four laminate configurations at -157°C, room temperature, and 316°C.

The composite sandwich beam compressive specimens were tested in a 533,787 N (120,000 lbf) capacity Baldwin test machine. Specimens were tested to failure using a constant load rate which ranged from 444.8 N/min (100 lbf/min) to 533.79 N/min (1200 lbf/min) depending on the laminate. A skematic diagram of a beam specimen loaded in four-point bending is shown in Figure 10. The beam was simply supported on rollers 48.26 cm (19.00 in) apart. A vertical load was applied to the beam at two locations on the top composite flange. The locations were 10.16 cm (4.00 in) apart and symmetric about the beam's center. A loaded beam specimen is shown in Figure 11. Stress concentrations at

---

*Strain rosettes for 316°C test laminates were aligned differently. The rosettes were oriented at -45°, 0°, and +45° with the load axis.

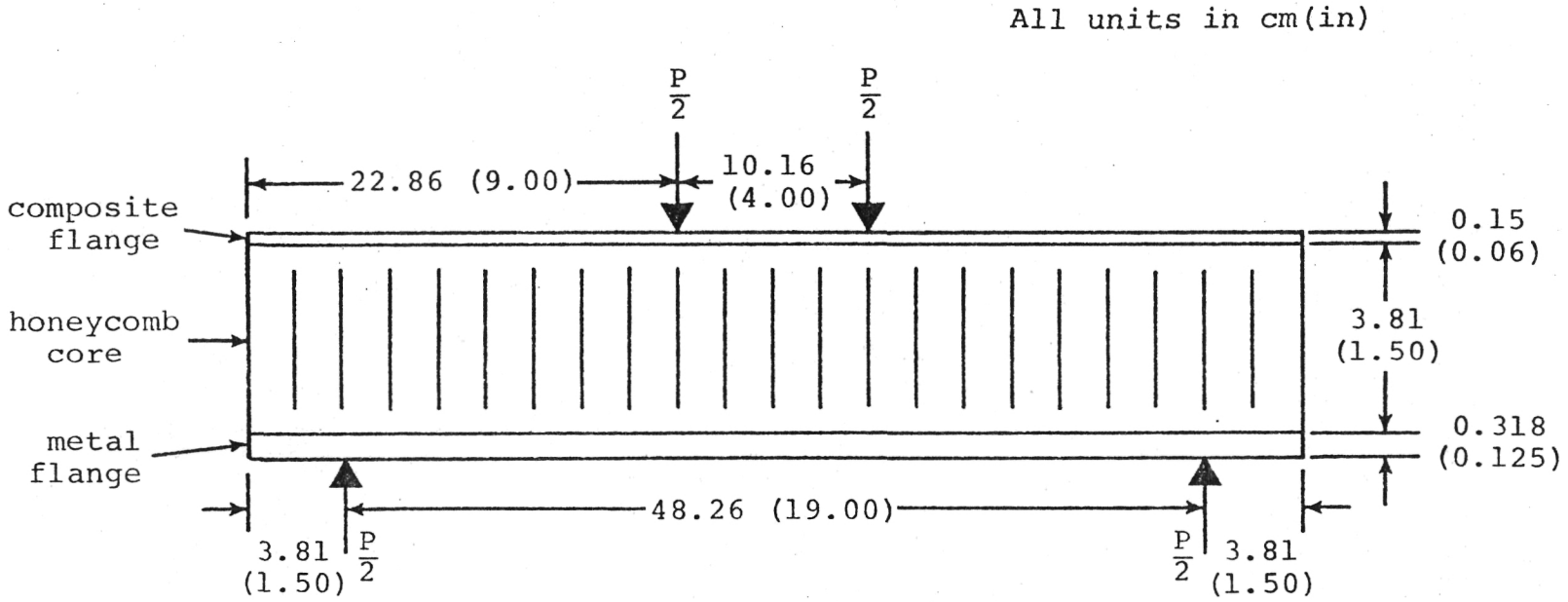

Figure 10. Schematic of Sandwich Beam Specimen Loaded in Four-Point Bending

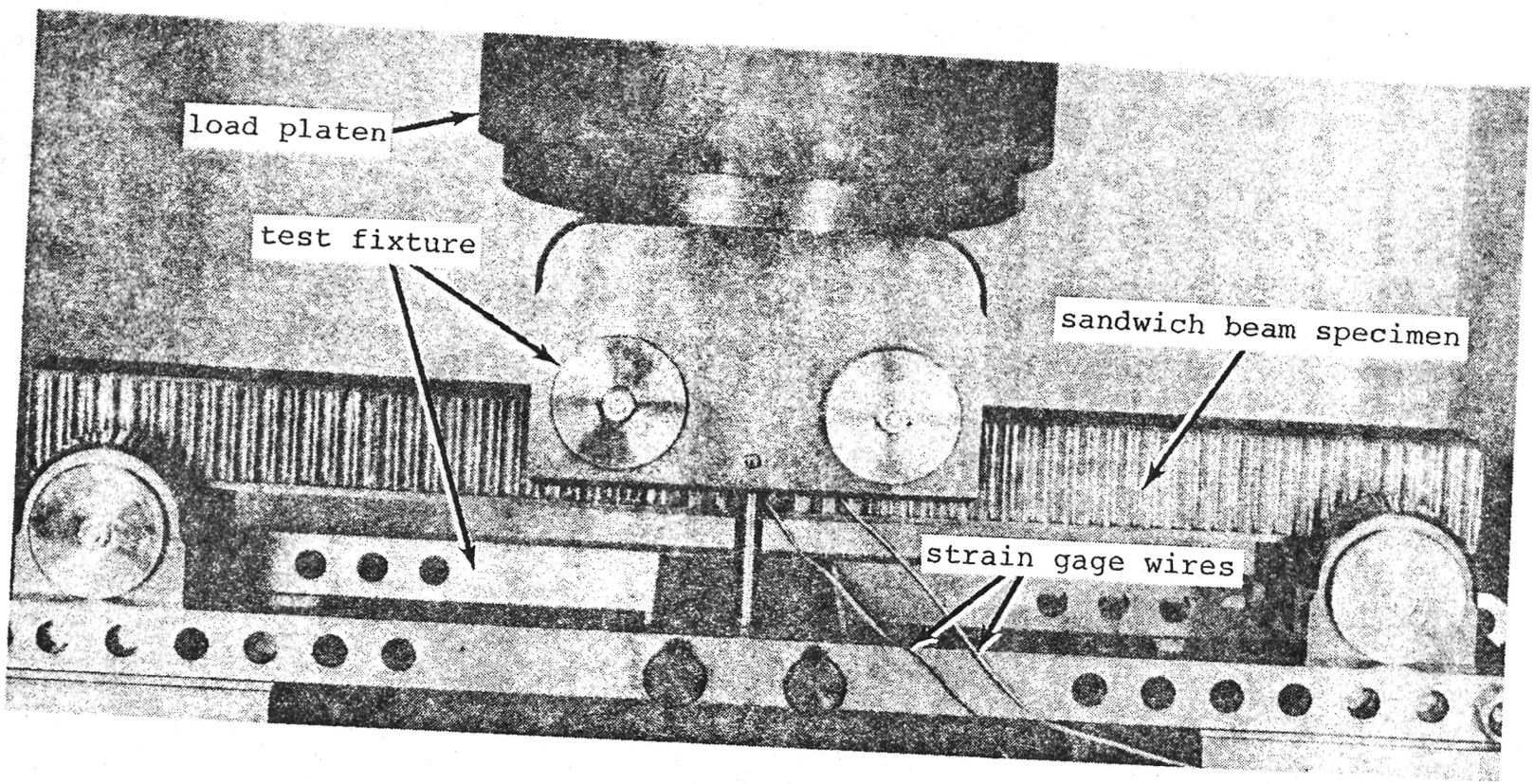

Figure 11. Typical Sandwich Beam Specimen Loaded in Four-Point Bending

load points were reduced by applying the load over a 6.45 cm^2 (1.00 in^2) area. Also, mylar load pads, 0.05 cm (0.02 in) thick, were used to reduce stress concentrations. Strain data were measured using foil-type strain gages mounted in the center of the composite flange. The $[0_8]$ and $[90_8]$ beam specimens had strain gages oriented at 0° and 90° with the load axis; the $[(\pm 45)_2]_s$ and $[0/\pm 45/90]_s$ beam specimens had strain rosettes oriented at 0°, 45°, and 90° with the load axis. All data were recorded using an automatic multi-channel data acquisition system. Twelve beam compressive tests were performed: three tests for each of the four laminate configurations.

The 2024-T3 sandwich beam compressive specimens were also tested in the Baldwin test machine using a constant load rate to failure. Load was applied to these specimens using the previously described four-point bending technique. No mylar load pads were needed for these tests. The toughness of the aluminum flange did not require extra consideration for stress concentrations. Load and strain data were obtained for determining Young's modulus and Poisson's ratio values. Strain data were measured using foil-type strain gages mounted in the center of the top flange and oriented at 0° and 90° with the load axis. Three beam compressive tests were performed.

Chapter 5

EXPERIMENTAL RESULTS

The experimental part of this investigation consisted of forty-three tests. Twenty-eight tests on beam constituent specimens and fifteen compressive tests on sandwich beam specimens were performed. Material property data from all tests are presented in Tables 1 through 8. The ultimate axial stress, σ_x^u, and the ultimate axial strain, ε_x^u, are defined as the maximum values attained during the test, and Young's modulus, E, Poisson's ratio, ν, and shear modulus, G, are calculated from the initial linear region of the stress-strain curves. The results from the experimental program include: (1) compressive elastic properties for 5052 aluminum honeycomb, (2) tensile and compressive data for HTS/PMR-15, and (3) compressive elastic properties for 2024-T3 aluminum.

5.1 Beam Constituent Tests

5.1.1 5052 aluminum honeycomb compressive specimens

The 5052 aluminum honeycomb specimens were tested in compression to determine elastic material properties. The coordinate system used to describe honeycomb material is shown in Figure 12. The L direction indicates the ribbon direction of the honeycomb. The W direction is transverse to the ribbon direction, and the T direction is through the thickness of the honeycomb. Data were obtained for those properties not available in the literature, specifically Young's modulus values, E_L and E_W, and Poisson's ratio values, ν_{LW} and ν_{WL}. The

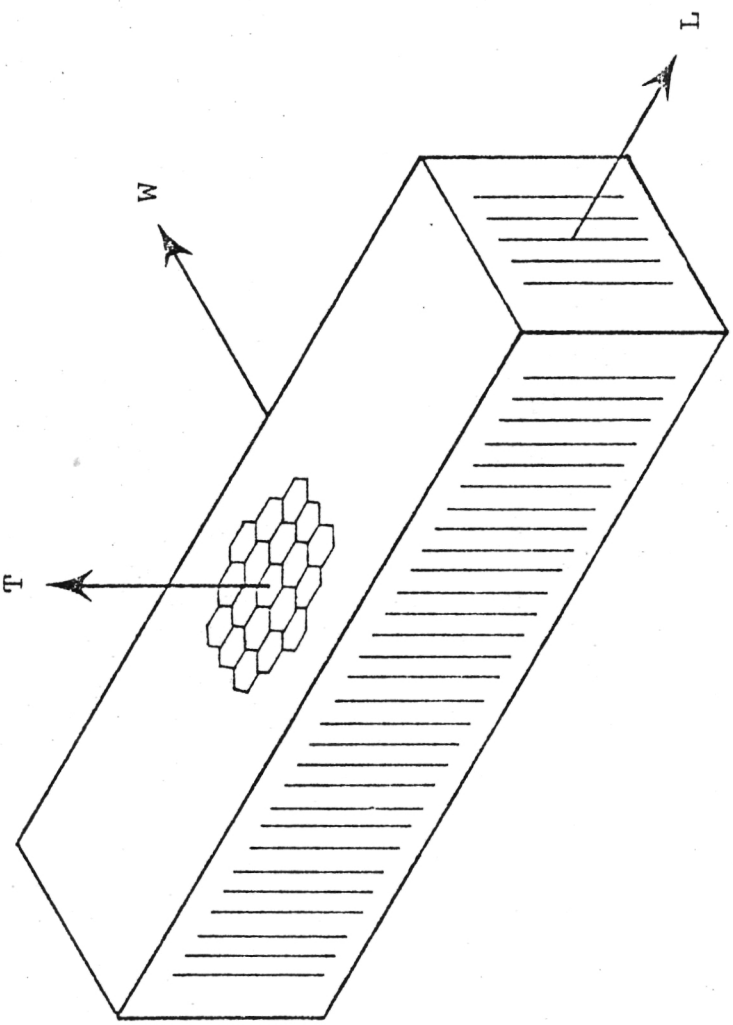

Figure 12. Honeycomb Coordinate System

data are presented in Table 1. Two tests each were performed for determining E_L, ν_{LW}, E_W, and ν_W.

Upon examining the honeycomb data (Table 1) two observations can be made: (1) the average Young's modulus for 5052 aluminum alloy is as much as five orders of magnitude higher than the E_L and E_W values, and (2) the ν_{LW} and ν_{WL} values are at least twice as large as the Poisson's ratio for 5052 aluminum alloy [34]. No further tests were conducted for these properties since the scatter in each reported property is no more than three percent.

Also shown in Table 1 is the ratio ν_{ij}/E_i for each test specimen. If the honeycomb is orthotropic

$$\frac{\nu_{LW}}{E_L} = \frac{\nu_{WL}}{E_W} \tag{5.1}$$

This is an assumption used in the computer analysis. All calculations are within a nine percent scatter indicating acceptable correlation. These experimental data verify this assumption.

5.1.2 Graphite/polyimide tensile specimens

Graphite/polyimide tensile data were obtained for room temperature, -157°C (-250°F), and 316°C (600°F) test environments. These data are tabulated in Tables 2 through 5, respectively. Failed tensile specimens from room temperature, -157°C, and 316°C tests are shown in Figures 13 through 15, respectively. A $[0_8]$ specimen is not shown in Figure 15 since these specimens splintered into several pieces upon failure. Figures 16 through 23 present σ_x-ε_x and σ_x-ε_y curves for

TABLE 1. 5052 ALUMINUM HONEYCOMB COMPRESSIVE DATA

Specimen Number	Young's Modulus, E_L, kPa (psi)	Poisson's Ratio, ν_{LW}	Young's Modulus, E_W, kPa (psi)	Poisson's Ratio, ν_{WL}	ν_{ij}/E_i, MPa^{-1} (psi^{-1})
AL-1	1751.3 (254.0)	1.08	-	-	0.617 (0.00425)
AL-2	1779.5 (258.1)	1.12	-	-	0.629 (0.00434)
AL-3	-	-	1068.0 (154.9)	0.71	0.665 (0.00458)
AL-4	-	-	1011.5 (146.7)	0.72	0.712 (0.00491)

TABLE 2. ROOM TEMPERATURE HTS/PMR-15 TENSILE TEST DATA

Laminate Configuration	Ultimate Stress, σ^u_x, MPa (ksi)	Ultimate Strain, ε^u_x, %	Young's Modulus, E_x, GPa (Msi)	Poisson's Ratio, ν_{xy}
$[0_8]$	1274.8 (184.9)	0.99	129.0 (18.71)	0.330
$[0_8]$	1434.1 (208.0)	1.08	132.9 (19.28)	0.332
$[90_8]$	24.34 (3.53)	0.30	8.20 (1.19)	0.010
$[90_8]$	42.75 (6.20)	0.54	8.27 (1.20)	0.013
$[(\pm45)_2]_s$	118.6 (17.21)	1.36	15.37 (2.23)	0.775
$[(\pm45)_2]_s$	100.1 (14.52)	1.09	13.72 (1.99)	0.738
$[0/\pm45/90]_s$	459.5 (66.64)	1.01	47.92 (6.95)	0.336
$[0/\pm45/90]_s$	441.7 (64.07)	0.95	47.64 (6.91)	0.325

TABLE 3. -157°C (-250°F) HTS/PMR-15 TENSILE TEST DATA

Laminate Configuration	Ultimate Stress, σ_x^u, MPa (ksi)	Ultimate Strain, ε_x^u, %	Young's Modulus, E_x, GPa (Msi)	Poisson's Ratio, ν_{xy}
$[0_8]$	1077.8 (156.33)	-*	123.7 (17.94)	-*
$[0_8]$	1146.6+ (166.3)	0.83+	127.4 (18.48)	0.349
$[90_8]$	33.30 (4.83)	0.34	10.07 (1.46)	0.062
$[90_8]$	28.54 (4.14)	0.32	9.31 (1.35)	0.054
$[(\pm 45)_2]_s$	95.08 (13.79)	0.52	18.89 (2.74)	0.688
$[(\pm 45)_2]_s$	110.8 (16.07)	0.85	16.75 (2.43)	0.676
$[0/\pm 45/90]_s$	238.8 (34.64)	0.54	44.95 (6.52)	0.366
$[0/\pm 45/90]_s$	464.6 (67.38)	0.23	43.23 (6.27)	0.263

*strain gage malfunction
+machine limit

TABLE 4. 316°C (600°F) HTS/PMR-15 TENSILE TEST DATA

Laminate Configuration	Ultimate Stress, σ_x^u, MPa (ksi)	Ultimate Strain, ε_x^u, %	Young's Modulus, E_x, GPa (Msi)	Poisson's Ratio, ν_{xy}
$[0_8]$	1285.2 (186.4)	0.97	132.1 (19.16)	0.355
$[0_8]$	1296.2 (188.0)	0.99	131.8 (19.11)	0.345
$[90_8]$	22.89 (3.32)	0.55	5.03 (0.73)	0.007
$[90_8]$	22.61 (3.28)	0.45	5.79 (0.84)	0.010
$[(\pm 45)_2]_s$	82.39 (11.95)	1.06*	9.10 (1.32)	0.766
$[(\pm 45)_2]_s$	65.64 (9.52)	0.95*	8.27 (1.20)	0.671
$[0/\pm 45/90]_s$	438.0 (63.52)	0.96	46.06 (6.68)	0.358
$[0/\pm 45/90]_s$	451.2 (65.44)	1.04	44.26 (6.42)	0.321

*maximum readable strain

TABLE 5. SHEAR MODULUS DATA FOR HTS/PMR-15
(TENSILE TESTS)

Specimen Number	Test Temperature, °C (°F)	Shear Modulus, G_{12}, GPa (Msi)
13-45	RT*	4.44 (0.643)
14-45	RT*	3.95 (0.573)
11-45	316 (600)	2.61 (0.378)
12-45	316 (600)	2.46 (0.357)
24-45	-157 (-250)	5.28 (0.766)
25-45	-157 (-250)	5.00 (0.725)

*room temperature

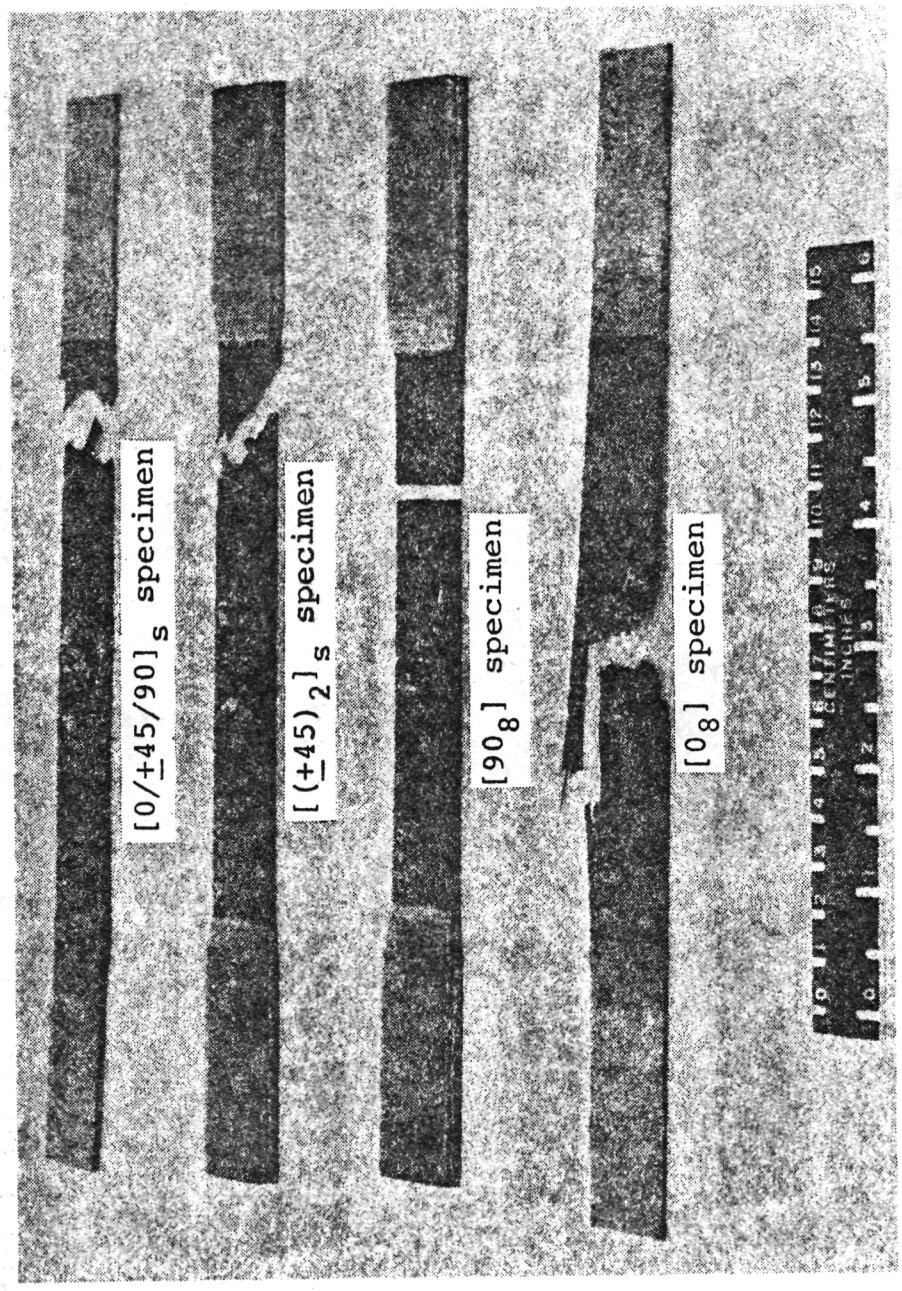

Figure 13. Failed Room Temperature HTS/PMR-15 Tensile Specimens

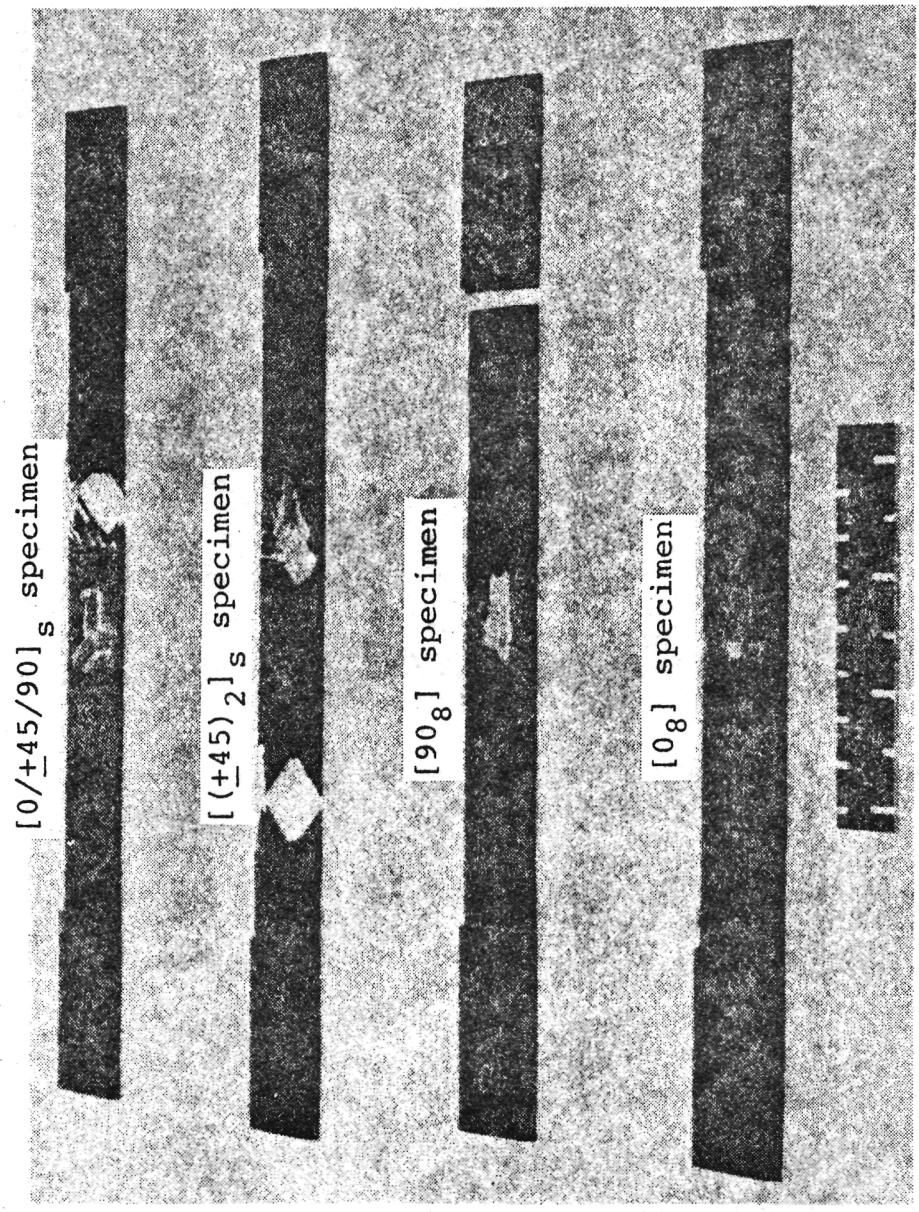

Figure 14. Failed -157°C (-250°F) HTS/PMR-15 Tensile Specimens

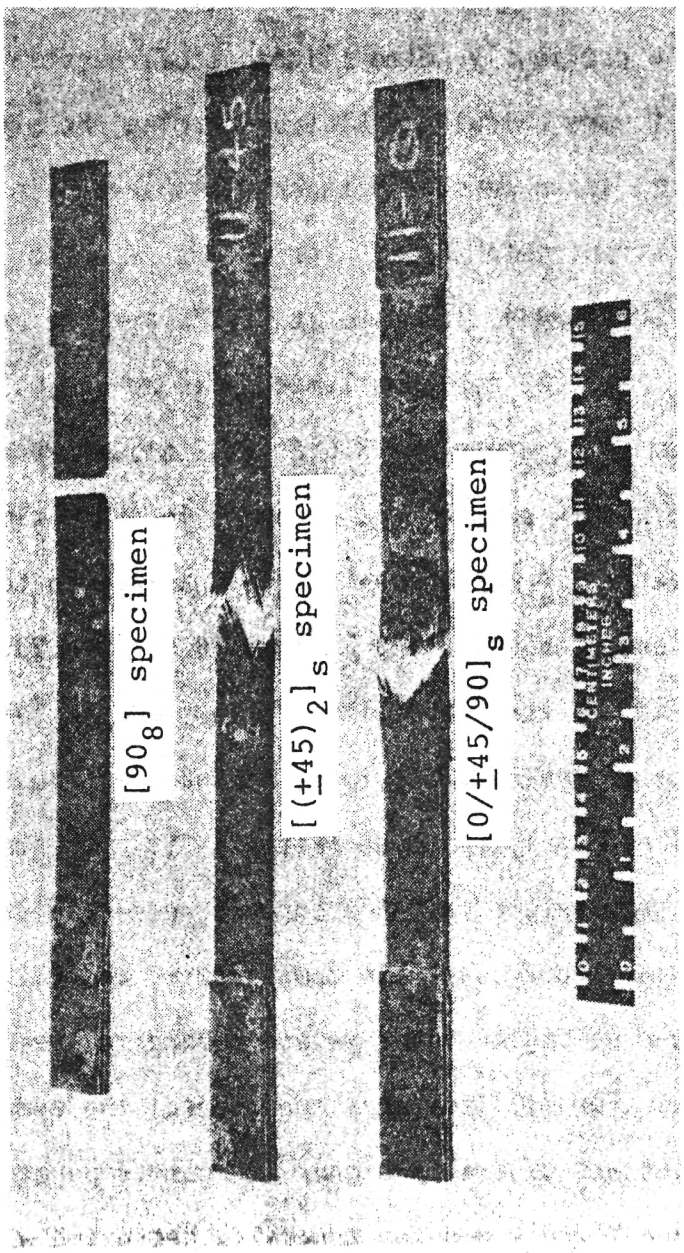

Figure 15. Failed 316°C (600°F) HTS/PMR-15 Tensile Specimens

representative laminates at the different test temperatures. A thin line is included with each σ_x-ε_x curve to indicate the initial slope of the curve (Figure 20). Transverse strain data were not obtainable directly at 316°C for the $[(\pm 45)_2]_s$ and $[0/\pm 45/90]_s$ laminates (Figures 21 and 23) because of the previously noted alignment of the strain rosettes. Poisson's ratio values were calculated by transforming the strain data. In general no more than seven percent scatter was observed in the elastic properties for replicate tests. The values reported for Poisson's ratio of a $[0/\pm 45/90]_s$ laminate at -157°C are the only exception. However, ν_{xy} = 0.263 for this laminate is an unusually low value compared to room temperature and 316°C results and may not be accurate. As expected, higher scatter was observed in the ultimate stress and ultimate strain data. In most cases scatter was within ten percent.

As shown in Tables 2 through 5 and Figures 16 through 23, test temperature does affect the tensile ultimate stress, ultimate strain, and elastic properties of graphite/polyimide laminates. The temperature dependence is controlled mainly by three factors: (1) thermal stresses due to the change in temperature from the cure (stress-free) temperature, (2) changes in material properties with temperature, and (3) material damage (such as micro-cracking or fiber-matrix debonding) resulting from thermal stresses. For all laminates considered, the average ultimate tensile stress was generally higher at room temperature than at -157°C or 316°C, and Young's modulus generally decreased with increasing temperature. The influence of test temperature will be discussed further in the following sections.

5.1.2.1 $[0_8]$ laminate

Figures 16 and 17 show σ_x-ε_x and σ_x-ε_y curves, respectively, for a $[0_8]$ laminate. For all test environments considered, the laminate exhibits nearly linear stress-strain behavior to failure with the test temperature affecting only the ultimate stress and ultimate strain. The σ_x-ε_x curves do show a small increase in Young's modulus with increasing strain. This is typical of unidirectional graphite composites [35]. Nevertheless, Young's modulus and Poisson's ratio are independent of temperature, a characteristic of fiber-dominated laminates. Average ultimate stress and ultimate strain values for -157°C and 316°C tests were lower than room temperature values. At the lower temperature thermal stresses and any resulting material degradation are greatest, whereas at the elevated temperature the thermal stresses are negligible but the properties of the matrix have changed. As expected, the $[0_8]$ configuration had the highest ultimate stress of all laminates tested.

5.1.2.2 $[90_8]$ laminate

The curves in Figures 18 and 19 for σ_x-ε_x and σ_x-ε_y, respectively, are for a $[90_8]$ laminate. The σ_x-ε_x curves at room temperature and 316°C exhibit initially linear response followed by nonlinear behavior. The σ_x-ε_x curve at -157°C is linear to failure. Significant differences are noted in the Young's modulus and Poisson's ratio values for the different test temperatures. Compared to the average room temperature property, Young's modulus is seventeen percent higher at -157°C and thirty-five percent lower at 316°C. Also, Poisson's ratio is more than three hundred percent higher at -157°C and thirty-three percent lower at

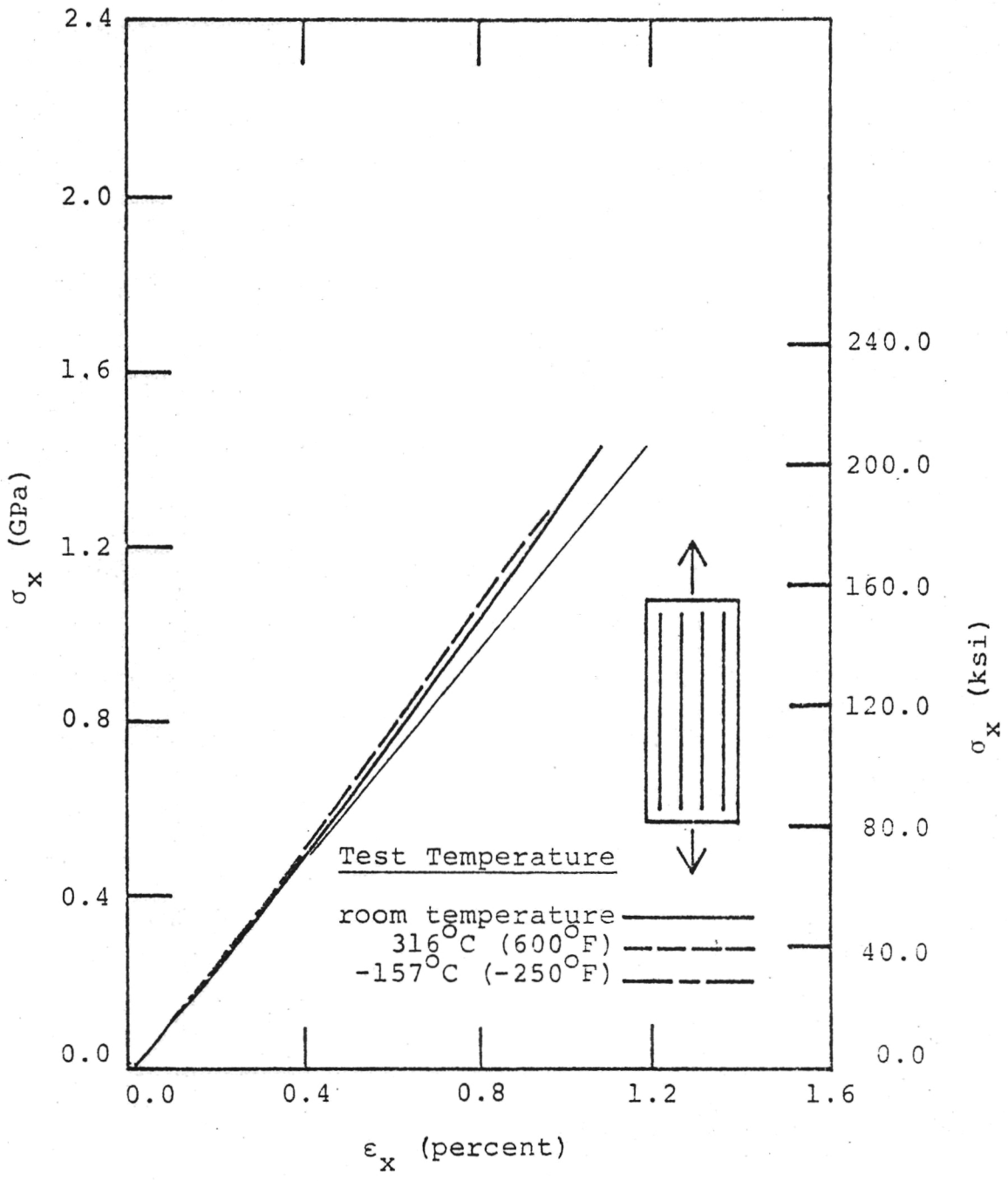

Figure 16. Comparison of Tensile σ_x - ε_x Behavior for $[0_8]$ HTS/PMR-15 at Different Test Temperatures

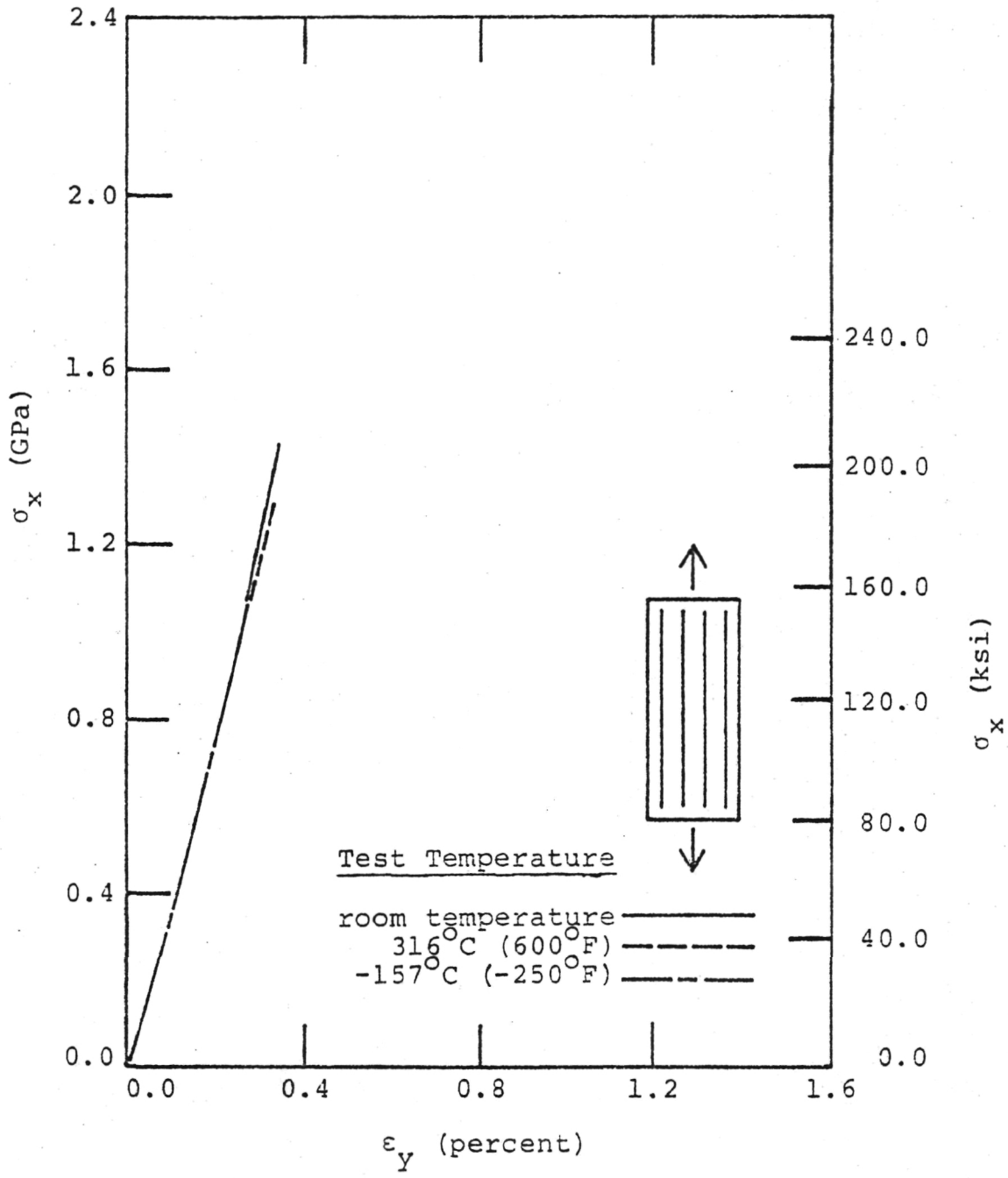

Figure 17. Comparison of Tensile σ_x - ε_y Behavior for $[0_8]$ HTS/PMR-15 at Different Test Temperatures

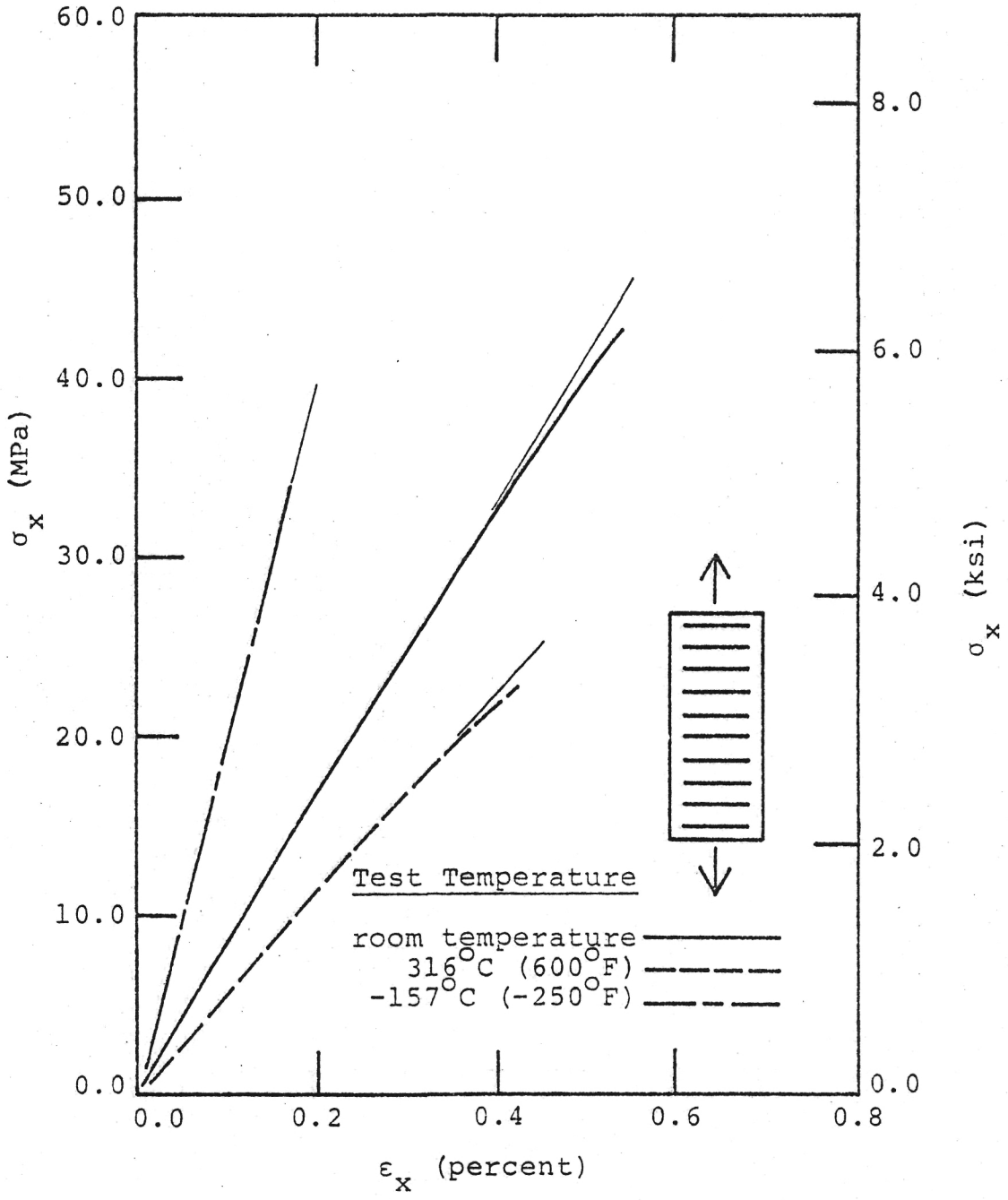

Figure 18. Comparison of Tensile σ_x - ε_x Behavior for $[90_8]$ HTS/PMR-15 at Different Test Temperatures

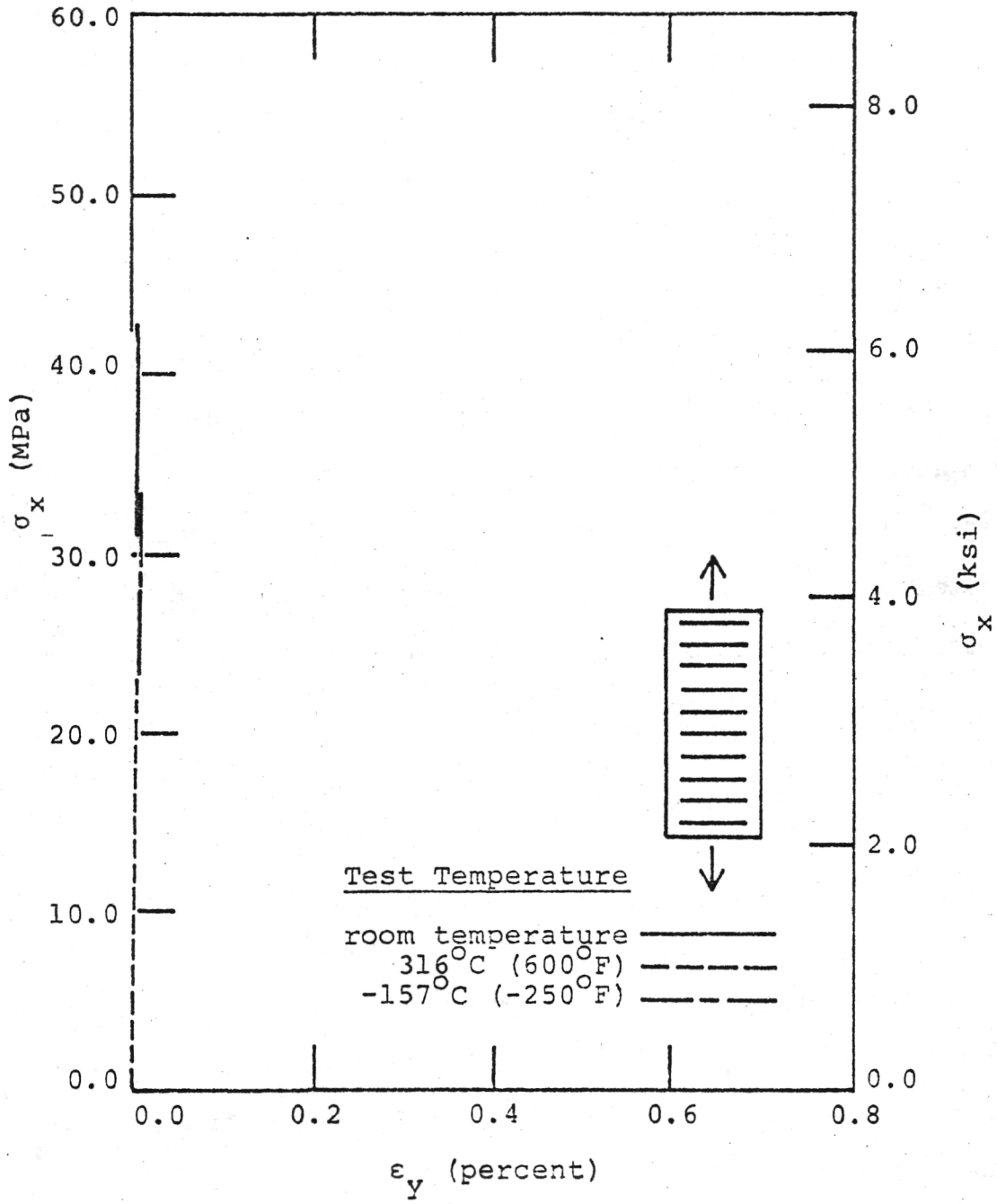

Figure 19. Comparison of Tensile σ_x - ε_y Behavior for $[90_8]$ HTS/PMR-15 at Different Test Temperatures

316°C than the average room temperature value. This type of behavior is characteristic of polyimide resins and is expected for this matrix-dominated laminate [36]. Average ultimate stress values at -157°C and 316°C were eight percent and thirty-two percent lower respectively, than the room temperature ultimate stress. The ultimate stress of the $[90_8]$ configuration was, as expected, the lowest of the laminates tested. The average ultimate strain at -157°C was twenty-one percent lower than the room temperature average; however, the average ultimate strain at 316°C was nineteen percent higher than the room temperature average. This variation of average ultimate strain with temperature is consistent with the variation of Young's modulus with temperature for this laminate. Compared to room temperature behavior, a higher (or lower) Young's modulus would cause a lower (or higher) strain response for a given stress level. For the corresponding tangent moduli, this behavior continues in the material nonlinear range resulting in the observed ultimate strain response.

5.1.2.3 $[(\pm 45)_2]_s$ laminate

Figures 20 and 21 present σ_x-ε_x and σ_x-ε_y curves, respectively, for a $[(\pm 45)_2]_s$ laminate. Although initially linear, these σ_x-ε_x curves showed the greatest nonlinearity of all tensile data obtained. Again, differences in elastic properties for the different test temperatures were observed. Compared to room temperature properties, Young's modulus was twenty-two percent higher and Poisson's ratio was ten percent lower at -157°C. Also, Young's modulus was forty percent lower and Poisson's ratio was five percent lower at 316°C. Differences less than ten

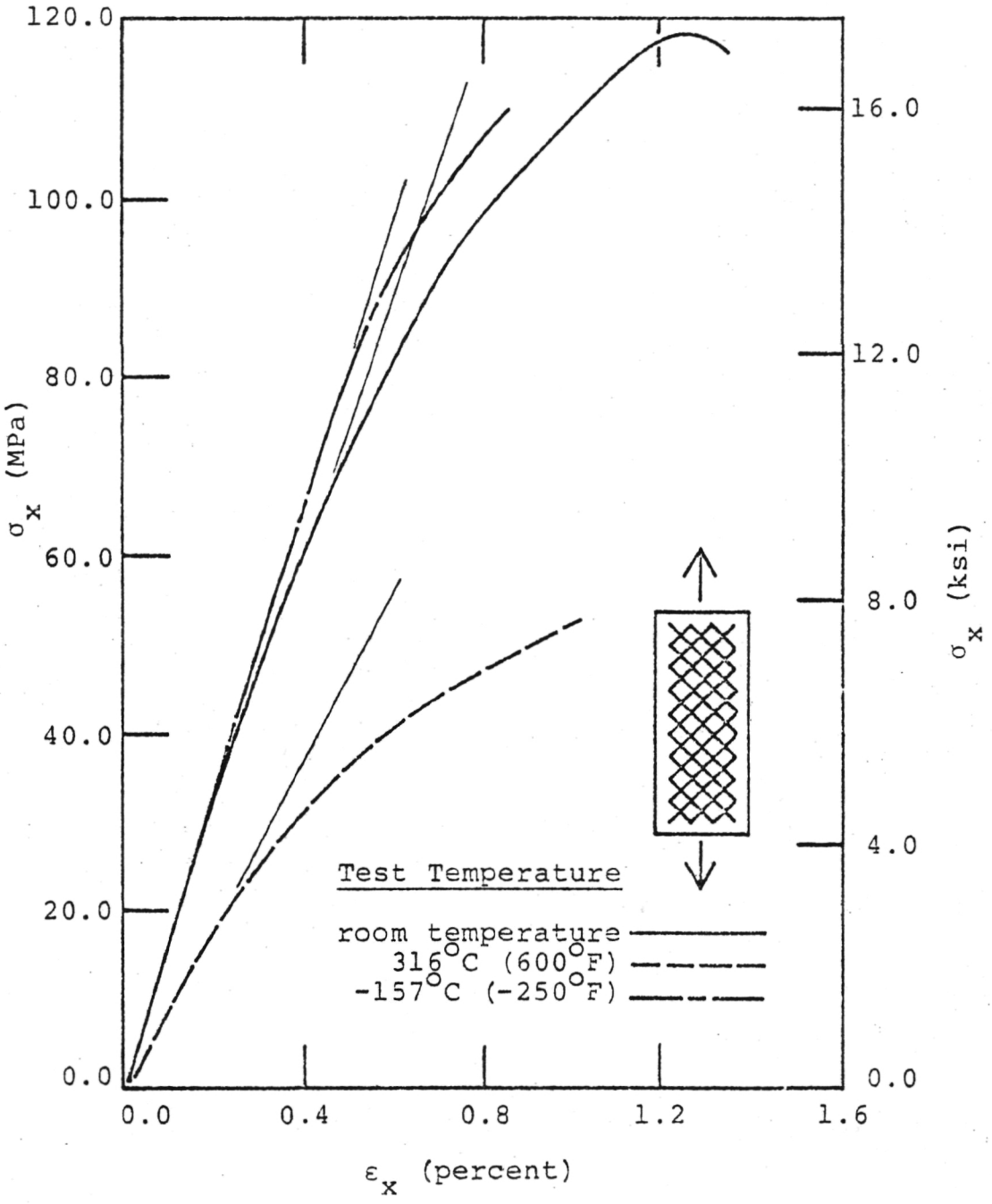

Figure 20. Comparison of Tensile σ_x - ε_x Behavior for $[(\pm 45)_2]_s$ HTS/PMR-15 at Different Test Temperatures

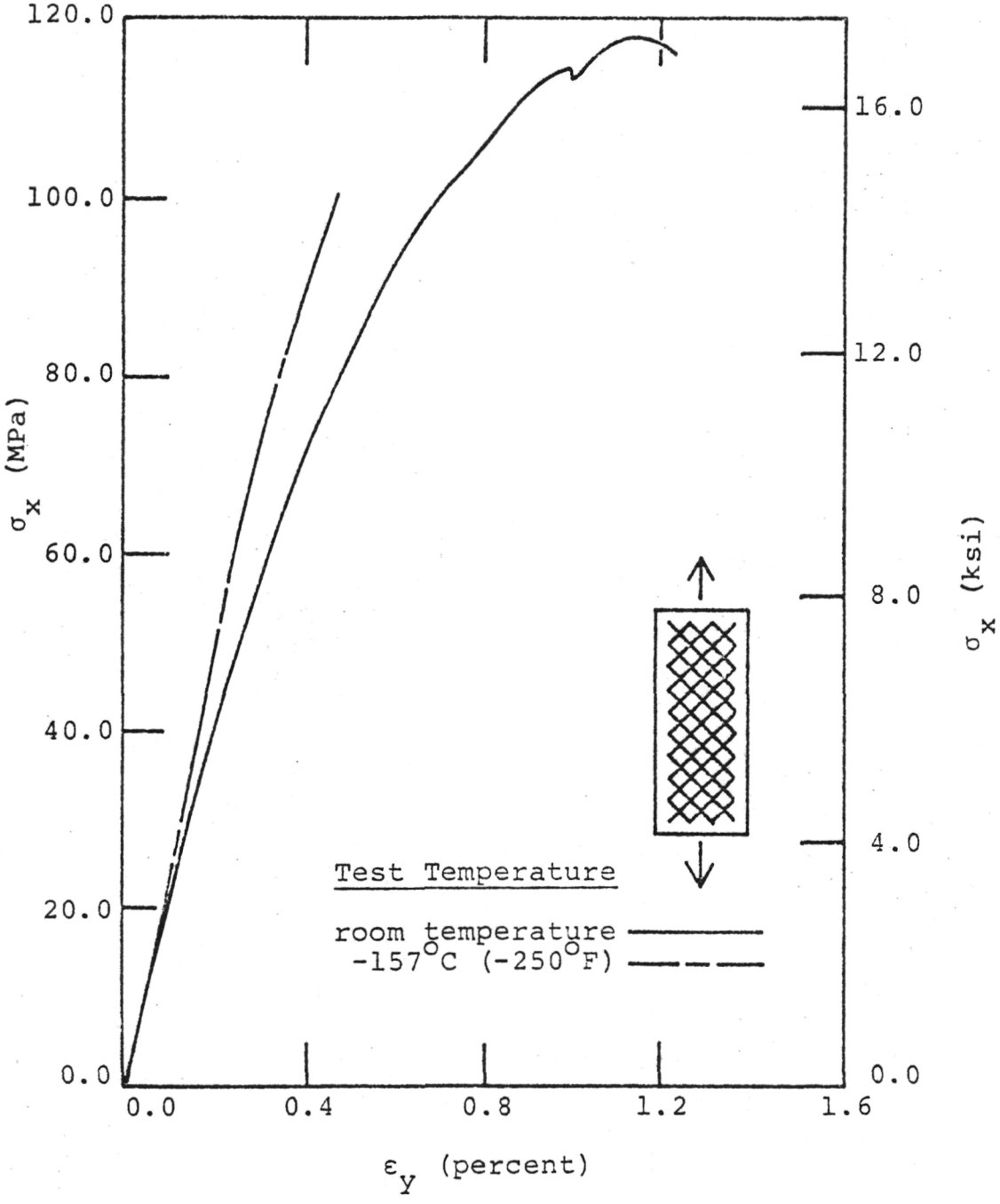

Figure 21. Comparison of Tensile σ_x - ε_y Behavior for $[(\pm 45)_2]_s$ HTS/PMR-15 at Different Test Temperatures

percent may be attributed to experimental scatter. Young's modulus values for the $[(\pm 45)_2]_s$ laminate at -157°C and 316°C are affected similarily to the $[90_8]$ laminate at these temperatures. However, Poisson's ratio for the $[(\pm 45)_2]_s$ laminate at these temperatures is affected differently from the $[90_8]$ laminate. These differences may be caused by material degradation in this extreme temperature. Average ultimate stress and ultimate strain values for the $[(\pm 45)_2]_s$ laminate differ for different test temperatures. Compared to the room temperature data, σ_x^u is six percent lower at -157°C and thirty-two percent lower at 316°C. This variation is nearly equal to that observed for σ_x^u of a $[90_8]$ laminate. Axial strain at failure was not recorded for this laminate at 316°C because the strain exceeded the range of the data acquisition system. The ε_x^u at -157°C was forty-four percent lower than the room temperature average. This is also similar to the $[90_8]$ behavior.

The linear stress-strain data from the $[(\pm 45)_2]_s$ laminate were used to calculate G_{12} for the graphite/polyimide system [37]. The data are presented in Table 5. Average G_{12} values were twenty-three percent higher at -157°C and forty percent lower at 316°C than the room temperature value. The variation with temperature for this property is similar to the previously explained variation with temperature of Young's modulus for a $[90_8]$ laminate.

5.1.2.4 $[0/\pm 45/90]_s$ laminate

The curves in Figures 22 and 23 of σ_x-ε_x and σ_x-ε_y, respectively, are for a $[0/\pm 45/90]_s$ laminate. This laminate exhibits linear stress-

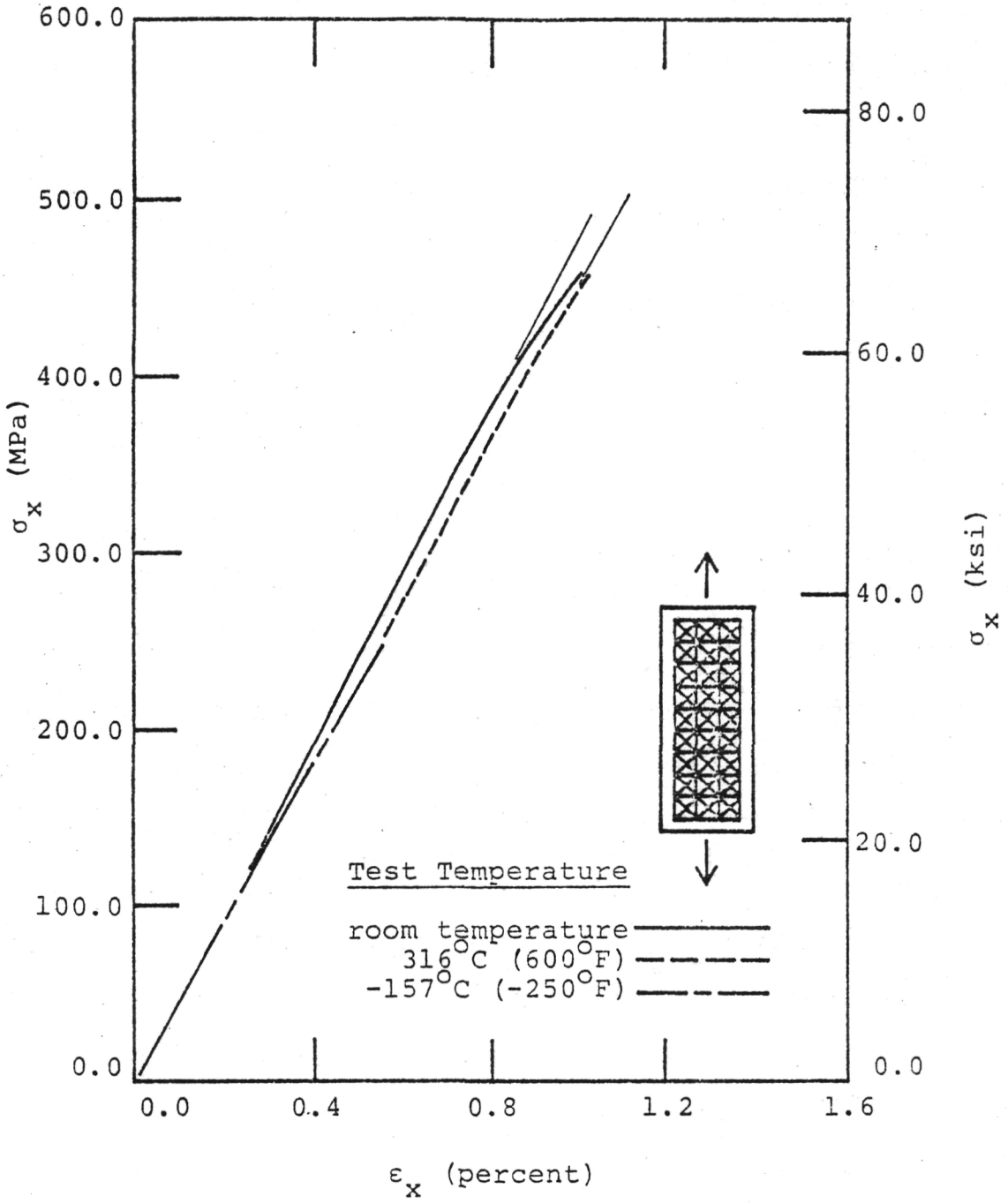

Figure 22. Comparison of Tensile σ_x - ε_x Behavior for $[0/\pm45/90]_s$ HTS/PMR-15 at Different Test Temperatures

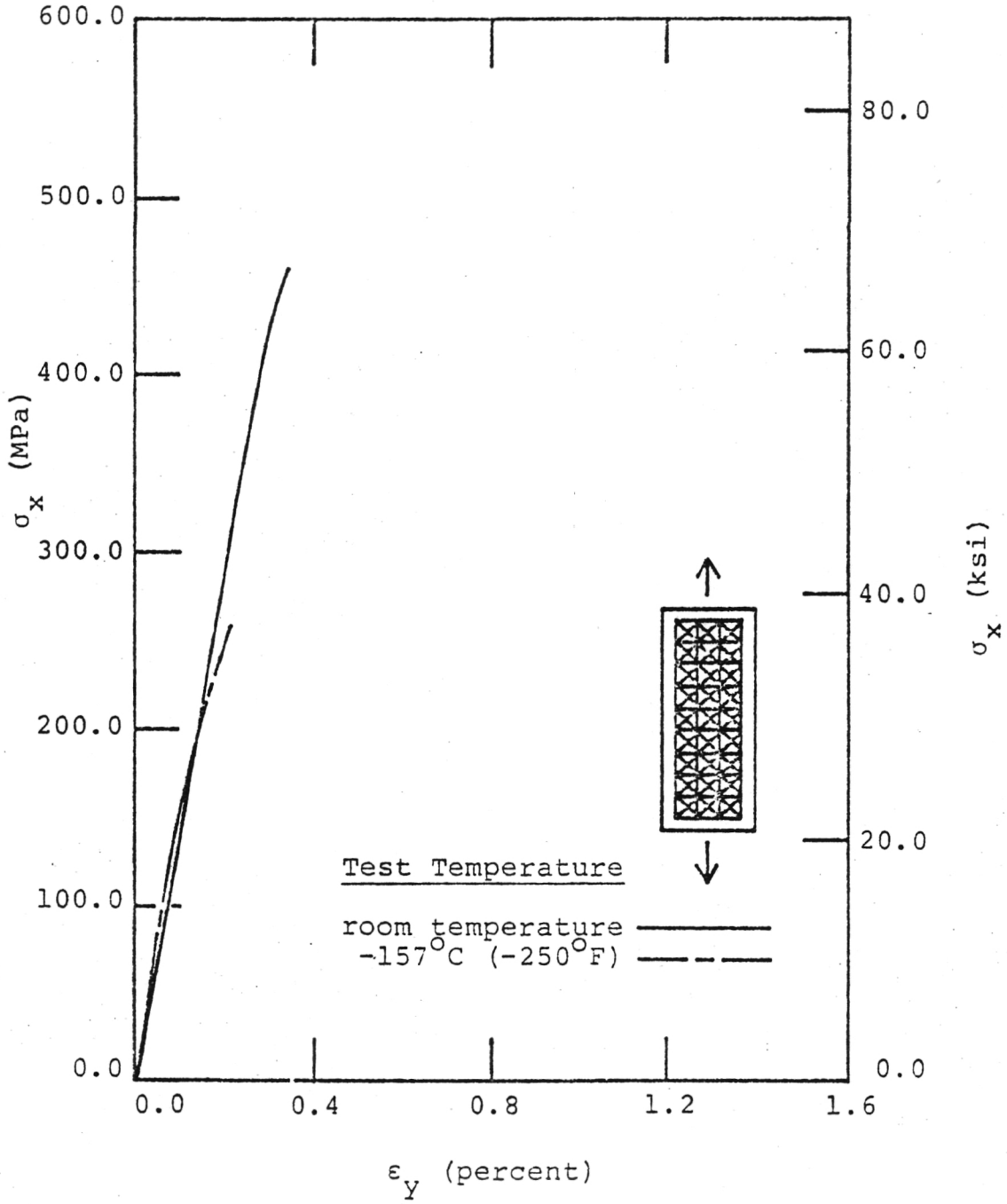

Figure 23. Comparison of Tensile σ_x - ε_y Behavior for $[0/\pm45/90]_s$ HTS/PMR-15 at Different Test Temperatures

strain behavior to failure for the -157°C and 316°C test temperatures. The room temperature test exhibits some nonlinearity just prior to failure. The Young's modulus and Poisson's ratio values for this laminate are independent of temperature. Average ultimate stress and ultimate strain values are approximately equal for room temperature and 316°C tests. The corresponding values of σ_x^u and ε_x^u at -157°C are twenty-two percent and sixty-one percent lower, respectively. These lower values may be caused by failure of the matrix due to the thermal stresses developed at this extreme temperature.

5.1.2.5 ν_{ij}/E_i comparisons

Comparisons of ν_{12}/E_1 and ν_{21}/E_2 were made at each test temperature. The values of ν_{12} and E_1 were obtained from the $[0_8]$ laminate, and the ν_{21} and E_2 values were obtained from the $[90_8]$ laminate. Although the graphite/polyimide system has orthotropic material symmetry, poor correlation between these values was observed for all test conditions. The source of the differences may be the value of ν_{21}. In all cases this value is small and may not be within the accuracy of the test procedure. Variations of ±0.001 are negligible for ν_{12} but significant for ν_{21}. Hence, the sensitivity of ν_{21} combined with the accuracy of the data may have influenced the ν_{ij}/E_i comparison.

5.2 Sandwich Beam Tests

5.2.1 Graphite/polyimide compressive specimens

Graphite/polyimide compressive data are presented in Tables 6 and 7. Typical failed beam specimens are shown in Figures 24 through 28.

TABLE 6. ROOM TEMPERATURE HTS/PMR-15 COMPRESSIVE TEST DATA

Laminate Configuration	Ultimate Stress, σ_x^u, MPa (ksi)	Ultimate Strain, ε_x^u, %	Young's Modulus, E_x, GPa (Msi)	Poisson's Ratio, ν_{xy}
$[0_8]$	1281.7 (185.9)	1.16	122.2 (17.73)	0.374
$[0_8]$	1270.0 (184.2)	1.19	119.0 (17.26)	0.353
$[0_8]$	1344.5 (195.0)	1.33	120.1 (17.42)	0.398
$[90_8]$	220.6 (32.00)	2.63	10.20 (1.48)	0.016
$[90_8]$	211.7 (30.70)	2.60	9.52 (1.38)	0.027
$[90_8]$	208.4 (30.22)	1.48	11.79 (1.71)	0.014
$[(\pm 45)_2]_s$	187.7 (27.22)	2.76	16.55 (2.40)	0.507
$[(\pm 45)_2]_s$	136.5 (19.80)	1.78	16.06 (2.33)	0.793

TABLE 6 (continued)

Laminate Configuration	Ultimate Stress, σ_x^u, MPa (ksi)	Ultimate Strain, ε_x^u, %	Young's Modulus, E_x, GPa (Msi)	Poisson's Ratio, ν_{xy}
$[(\pm 45)_2]_s$	136.5 (19.80)	2.07	16.75 (2.43)	0.743
$[0/\pm 45/90]_s$	552.6 (80.15)	1.65	46.75 (6.78)	0.278
$[0/\pm 45/90]_s$	529.8 (76.84)	1.33	47.02 (6.82)	0.296
$[0/\pm 45/90]_s$	535.1 (77.61)	1.29	48.54 (7.04)	0.277

TABLE 7. ROOM TEMPERATURE SHEAR MODULUS FOR HTS/PMR-15 (COMPRESSIVE TESTS)

Specimen Number	Shear Modulus, G_{12}, GPa (Msi)
1-45	5.83 (0.846)
2-45	4.99 (0.724)
3-45	5.11 (0.742)

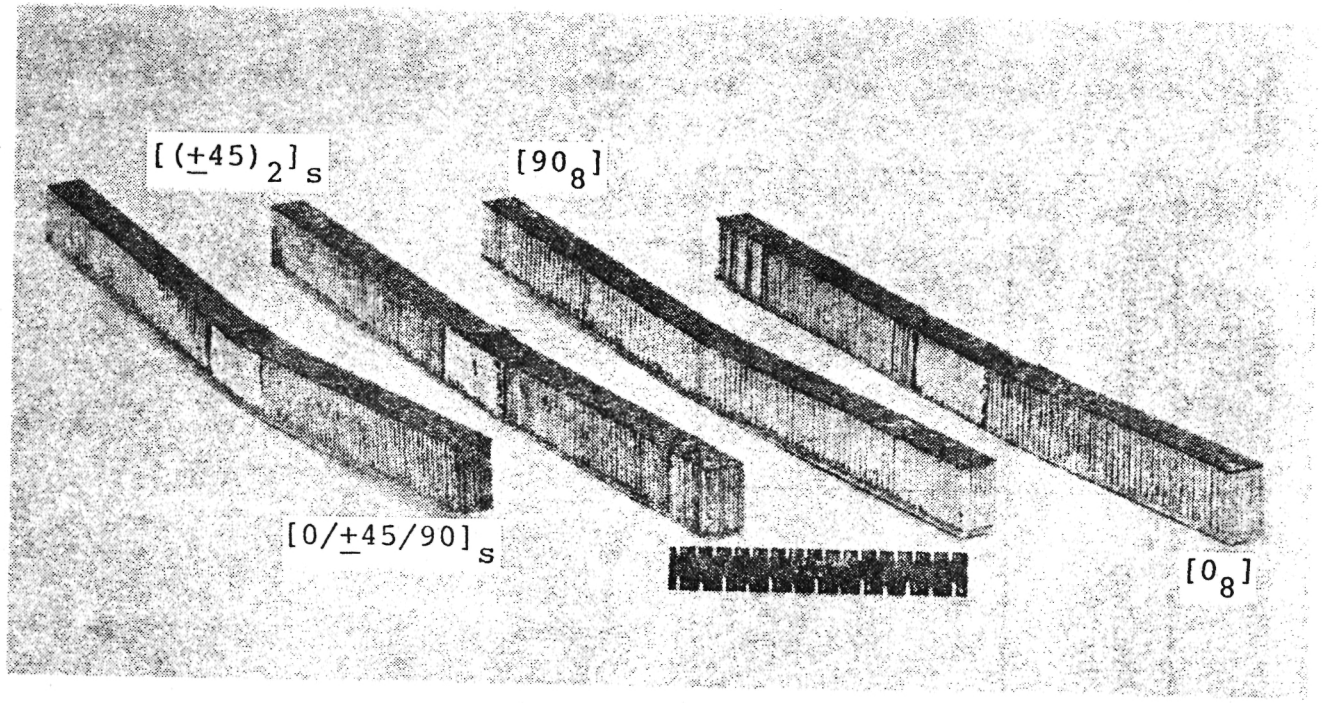

Figure 24. Failed Room Temperature HTS/PMR-15 Sandwich Beam Specimens

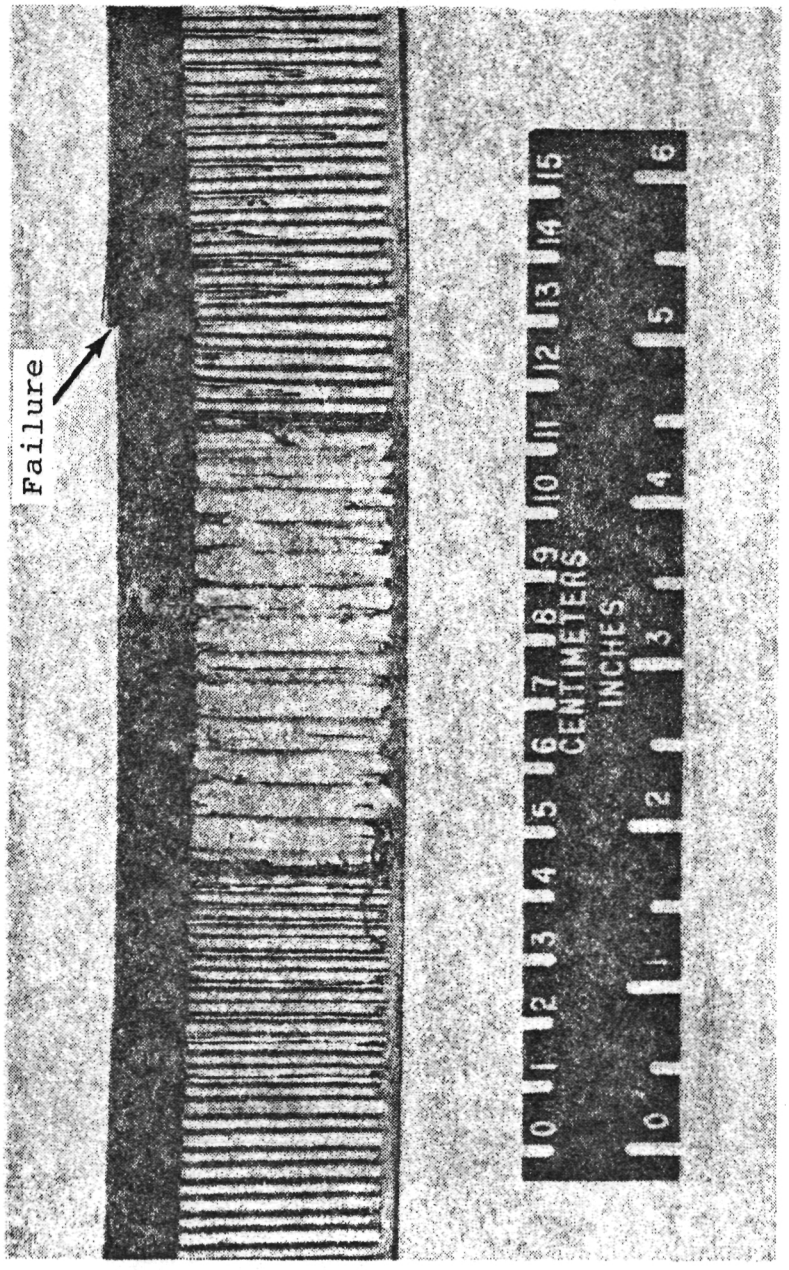

Figure 25. Failed Room Temperature $[0_8]$ HTS/PMR-15 Beam Specimen

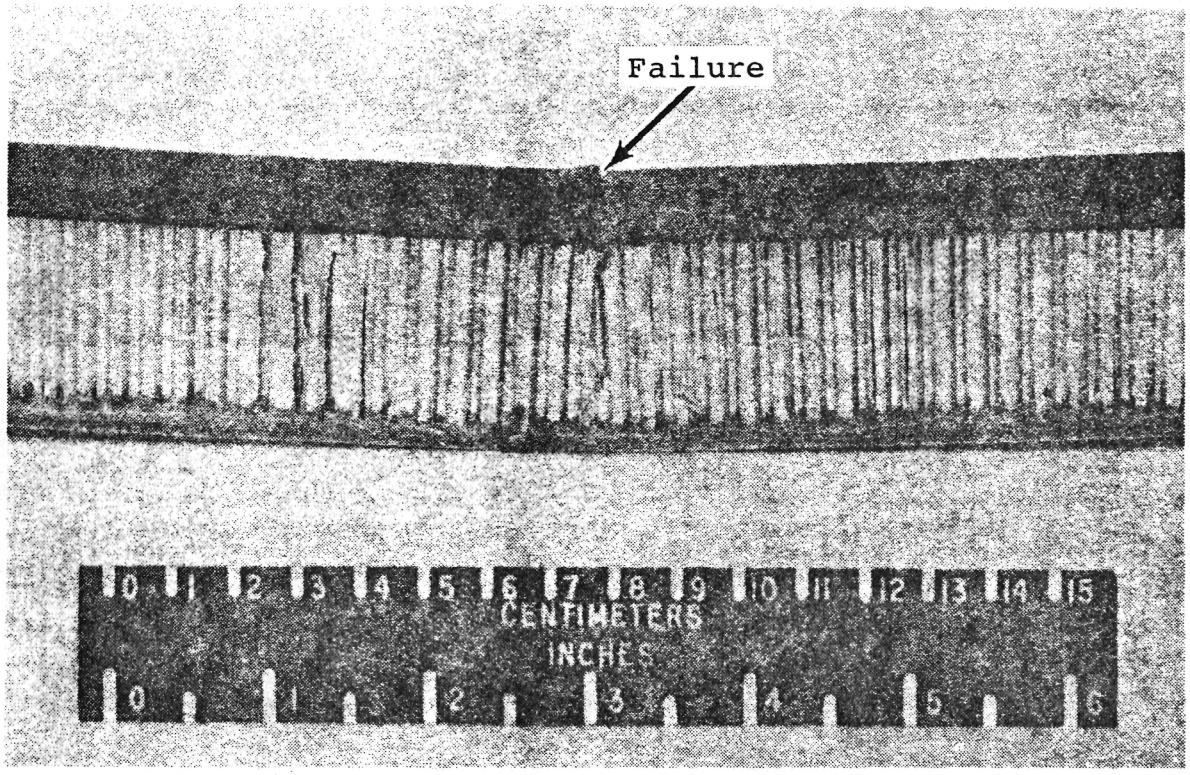

Figure 26. Failed Room Temperature [90_8] HTS/PMR-15 Beam Specimen

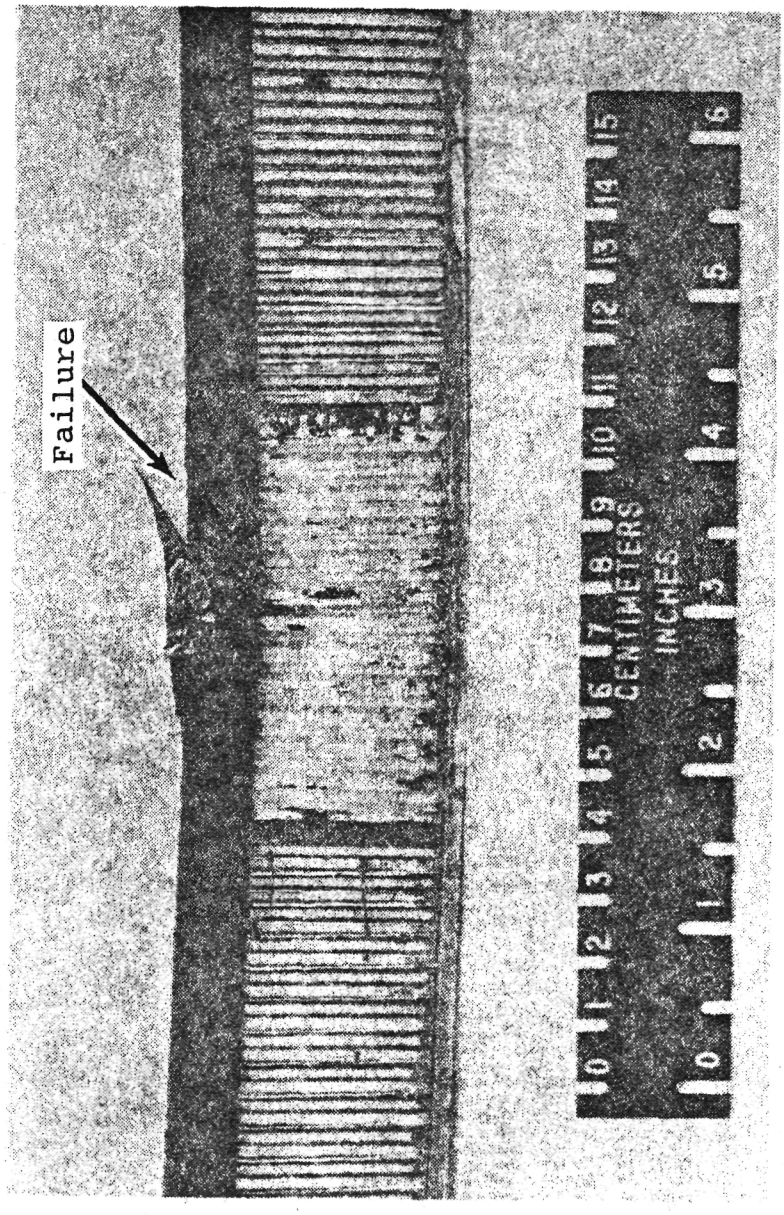

Figure 27. Failed Room Temperature $[(\pm 45)_2]_s$ HTS/PMR-15 Beam Specimen

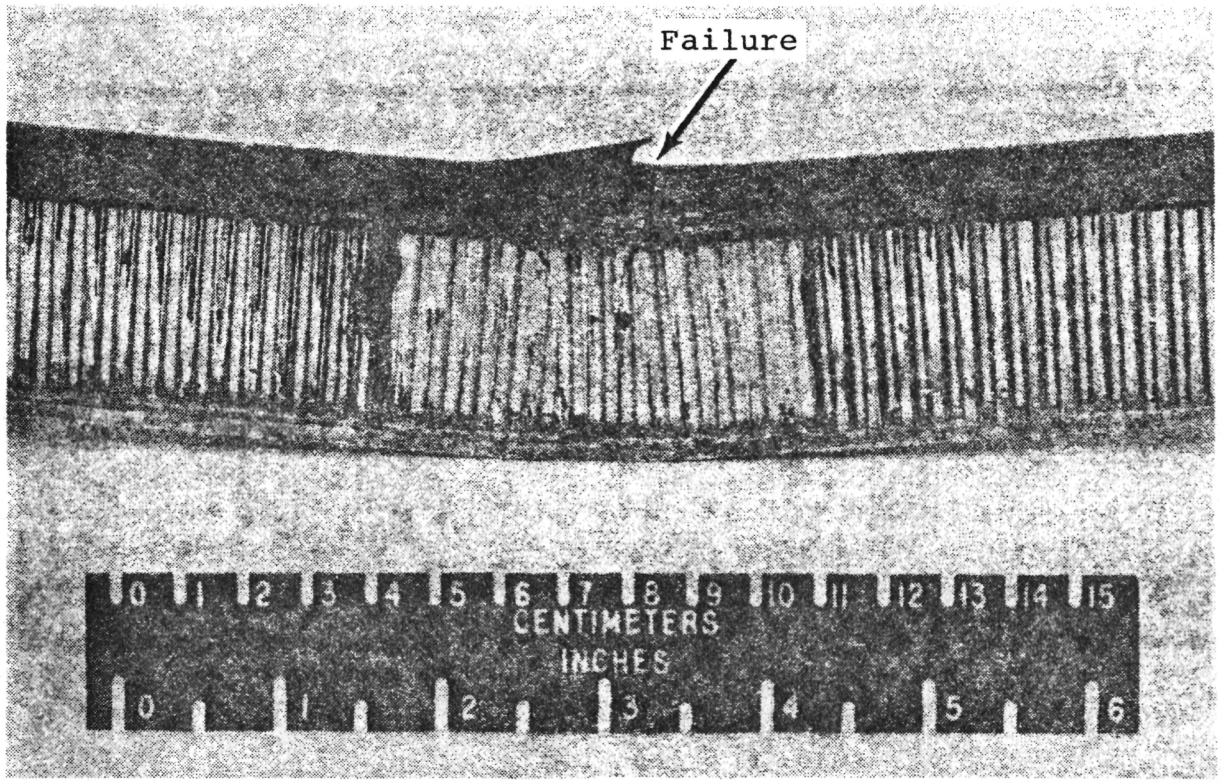

Figure 28. Failed Room Temperature $[0/\pm45/90]_s$ HTS/PMR-15 Beam Specimen

Unless otherwise indicated, all composite laminates failed in the test section of the beam. Observed modes of failure for these laminates were similar to the failure modes for epoxy and metal matrix beam specimens [27,38]. Stress-strain curves for each laminate configuration are shown in Figures 29 through 32. A thin line is included with each σ_x-ε_x curve to indicate the initial slope of the curve. The variation of Poisson's ratio with axial strain was also investigated for these compressive specimens. Poisson's ratio for a $[(\pm 45)_2]_s$ laminate increased as much as thirty percent with increasing axial strain. Minimal, if any, variation was observed for this property as a function of axial strain for the other laminates. Generally, Young's modulus, shear modulus, and Poisson's ratio values were within a twelve percent scatter. Exceptions are a $[90_8]$ laminate, $\nu_{xy} = 0.027$, and a $[(\pm 45)_2]_s$ laminate, $\nu_{xy} = 0.507$. Each of these values differs significantly from the corresponding replicate tests and may not be accurate. As expected, higher scatter was observed for the ultimate stress and ultimate strain data. In most cases scatter was within sixteen percent.

5.2.1.1 $[0_8]$ laminate

Figure 25 illustrates a detailed view of a $[0_8]$ sandwich beam failure. Although load pads were used, this laminate failed in bearing at the point of load application. Typical compressive stress-strain curves for axial and transverse strain are shown in Figure 29. The material behavior is initially linear but becomes nonlinear at higher strains. Unlike the tensile Young's modulus, the compressive Young's

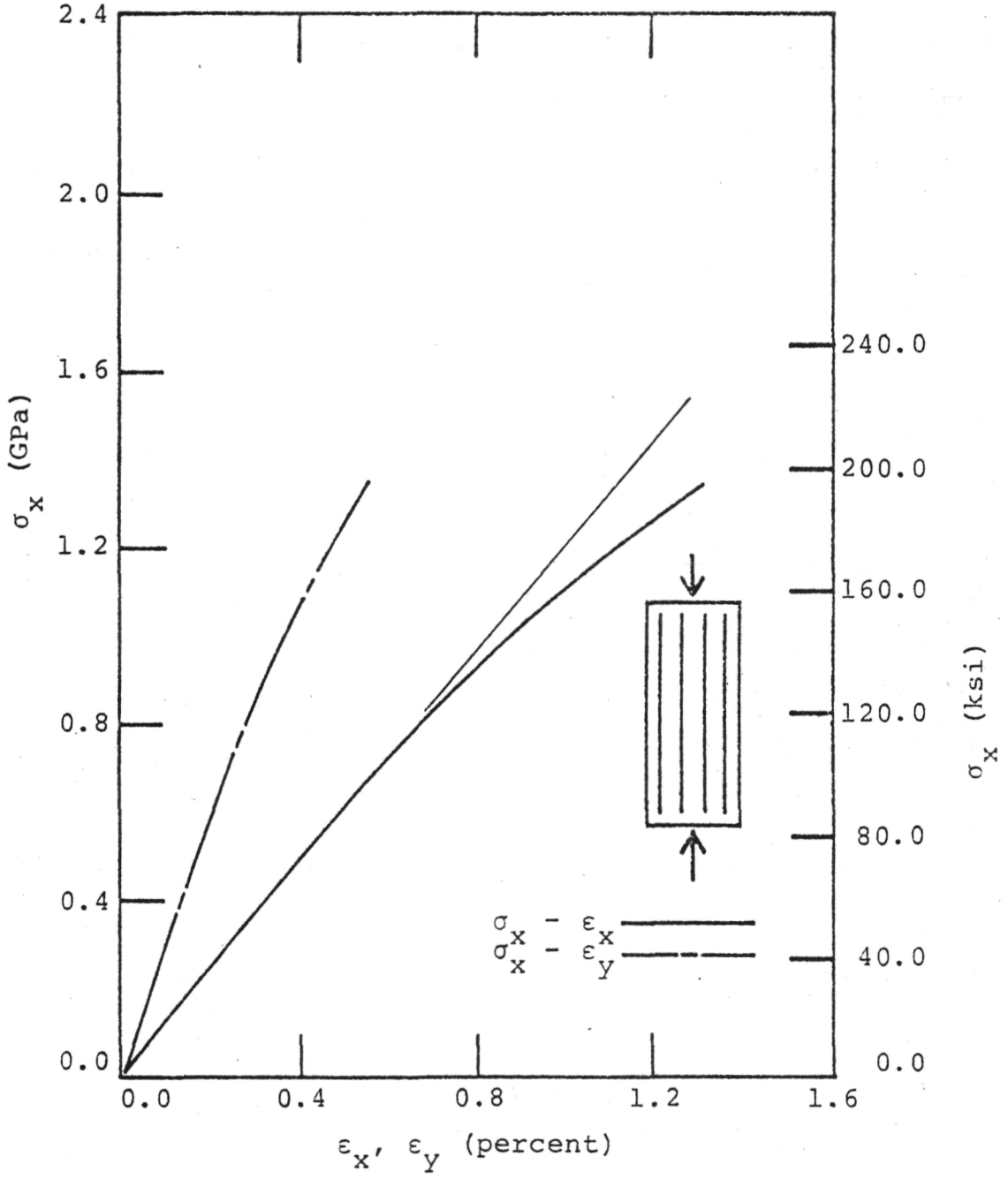

Figure 29. Room Temperature Compressive Stress-Strain Behavior for $[0_8]$ HTS/PMR-15.

modulus decreases with increasing axial strain. This tensile and compressive behavior is consistent with initial curvatures being present in the graphite fibers [21]. A tensile stress straightens the fibers and increases the laminate stiffness. A compressive stress adds to the fiber curvature thereby decreasing laminate stiffness. The average ultimate compressive stress for this laminate is the highest of the laminates considered as would be expected.

5.2.1.2 $[90_8]$ laminate

The test section of a $[90_8]$ beam specimen is shown in Figure 26. This laminate buckled causing failure. The honeycomb core was crushed at the point of composite failure due to the buckling of the laminate. Figure 30 presents compressive stress-strain data for this laminate. The σ_x-ε_x curve is initially linear but is nonlinear for most of the strain range. An unexpected result for this laminate was that the average ultimate compressive stress was not the lowest for the laminates considered. This will be discussed in the following section.

5.2.1.3 $[(\pm 45)_2]_s$ laminate

A portion of a $[(\pm 45)_2]_s$ beam specimen is shown in Figure 27. The composite laminate failed along a 0.785R (45°) axis with respect to the length of the beam. Ply delamination accompanied the crushing-type failure as seen in the figure. Stress-strain data are presented in Figure 31. The curves are initially linear but become nonlinear with increasing strain. Also, prior to failure the sudden decrease in stress indicates significant local damage. The laminate does, however, continue to strain considerably prior to total failure. This laminate

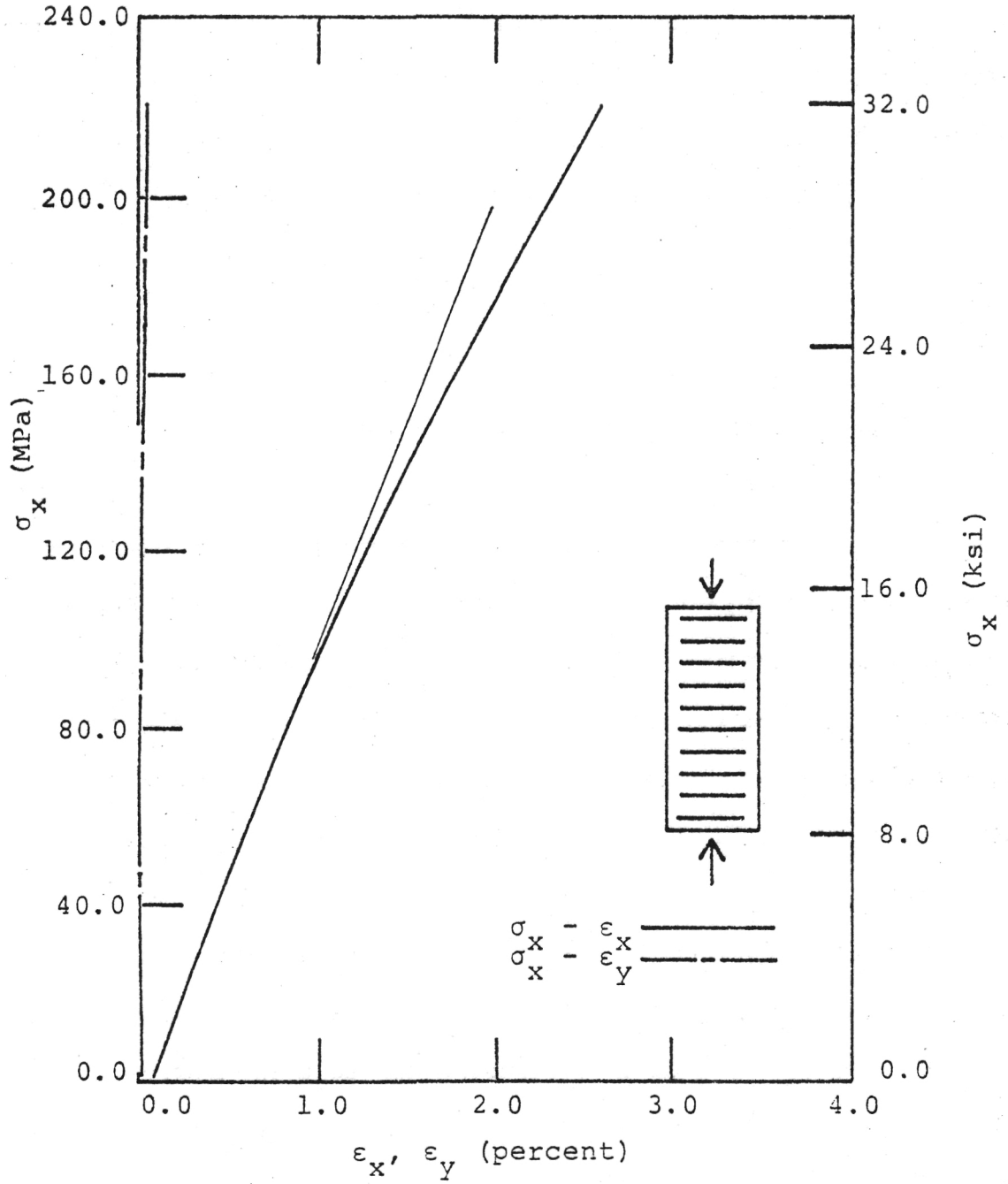

Figure 30. Room Temperature Compressive Stress-Strain Behavior for $[90_8]$ HTS/PMR-15.

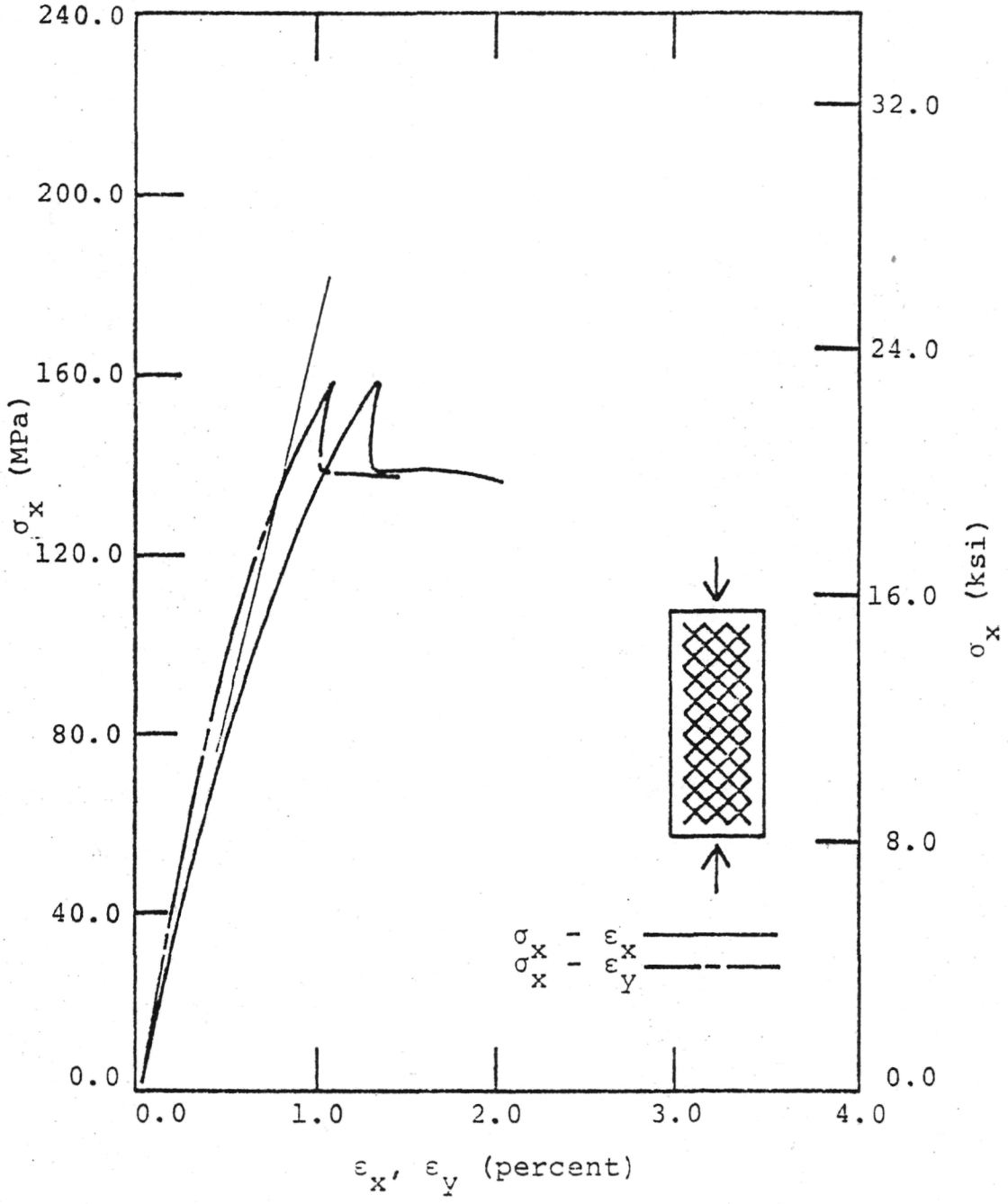

Figure 31. Room Temperature Compressive Stress-Strain Behavior for $[(\pm 45)_2]_s$ HTS/PMR-15.

had the lowest average ultimate compressive stress of the laminates tested. A detailed evaluation of the strain data provides a possible explaination for this behavior. Ultimate strains for the $[(\pm 45)_2]_s$ can be transformed from the laminate coordinate system to the natural coordinate system (Figure 5), and the transformed ultimate strains can then be compared with $[0_8]$ and $[90_8]$ ultimate strains. This comparison reveals that the transformed strain in the fiber direction at failure is greater than the ultimate axial strain for a $[0_8]$ laminate. Hence, the $[(\pm 45)_2]_s$ laminate may be governed by a maximum strain failure criterion.

Shear modulus values can be determined from the compressive tests of this laminate in the same manner used for the tensile tests [37]. The results of the calculations are shown in Table 7.

5.2.1.4 $[0/\pm 45/90]_s$ laminate

Figure 28 illustrates the test section of a $[0/\pm 45/90]_s$ beam specimen. A crushing-type failure mode accompanied by ply delamination was observed for this laminate. The stress-strain data are presented in Figure 32. Similar to the other laminates these curves are initially linear before becoming nonlinear.

5.2.1.5 ν_{ij}/E_i comparisons

Comparison of ν_{12}/E_1 and ν_{21}/E_2 was made for the compressive data. Similar to the tensile results, poor correlation exists between these compressive values. Any effects from a biaxial stress state may have influenced the transverse strain response. As detailed in the tensile data discussion, the sensitivity of ν_{21} combined with the accuracy of

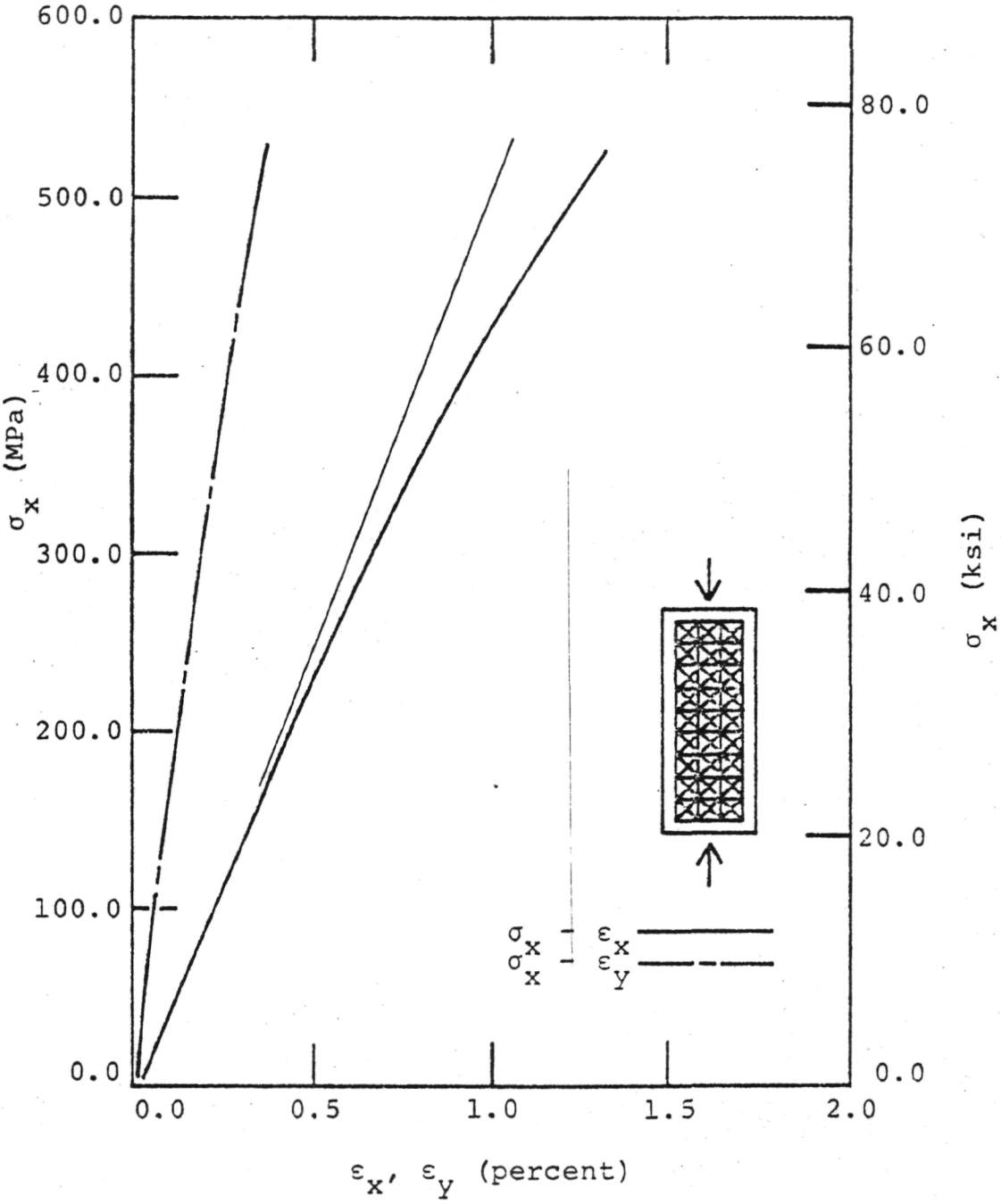

Figure 32. Room Temperature Compressive Stress-Strain Behavior for $[0/\pm45/90]_s$ HTS/PMR-15.

this property may have affected the ν_{ij}/E_i comparison.

5.2.2 2024-T3 aluminum compressive specimens

Compressive data for 2024-T3 aluminum are tabulated in Table 8, and a failed beam specimen is shown in Figure 33. The beam failed in core buckling in the region of maximum transverse shear stress. Due to this mode of failure, the ultimate stress and ultimate strain values for these specimens do not correspond to compressive strength and maximum obtainable strain, respectively, for this material. The σ_x^u and ε_x^u data are maximum observed values for each test. No more than two percent scatter was observed in these data. Typical stress-strain behavior are presented in Figure 34. The material behavior is linear throughout the test since all the observed stress levels are lower than the yield stress for this material. The Young's modulus data has a scatter of less than one percent, and the Poisson's ratio data has a scatter of no more than nine percent. Hence, all data from these beam specimens were within experimental scatter.

Average Young's modulus and Poisson's ratio obtained from these beam tests can be compared with documented aluminum compressive behavior [34]. The average observed Young's modulus is 72.95 GPa (10.58 Msi) compared to the documented value of 73.77 GPa (10.7 Msi). Also, the average Poisson's ratio for the present study is 0.311 while the documented value is 0.33. For both of these elastic properties the difference between observed and documented data is within normal experimental scatter. Hence, beam bending is an accurate method for determining elastic behavior of this material.

TABLE 8. ROOM TEMPERATURE 2024-T3 ALUMINUM COMPRESSIVE DATA

Specimen Number	Ultimate Stress, σ_x^u, MPa (ksi)	Ultimate Strain, ϵ_x^u, %	Young's Modulus, E, GPa (Msi)	Poisson's Ratio, ν
2024-1	230.3 (33.40)	0.32	72.53 (10.52)	0.282
2024-2	235.9 (34.21)	0.33	73.43 (10.65)	0.324
2024-3	229.7 (33.32)	0.32	72.81 (10.56)	0.328

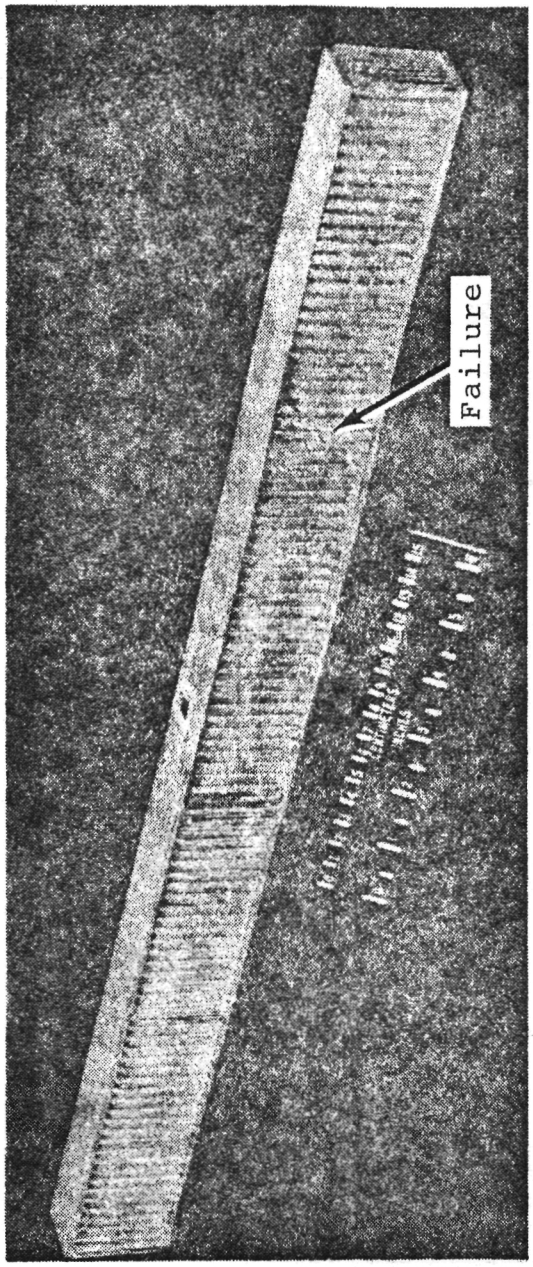

Figure 33. Failed Room Temperature 2024-T3 Aluminum Sandwich Beam Specimen

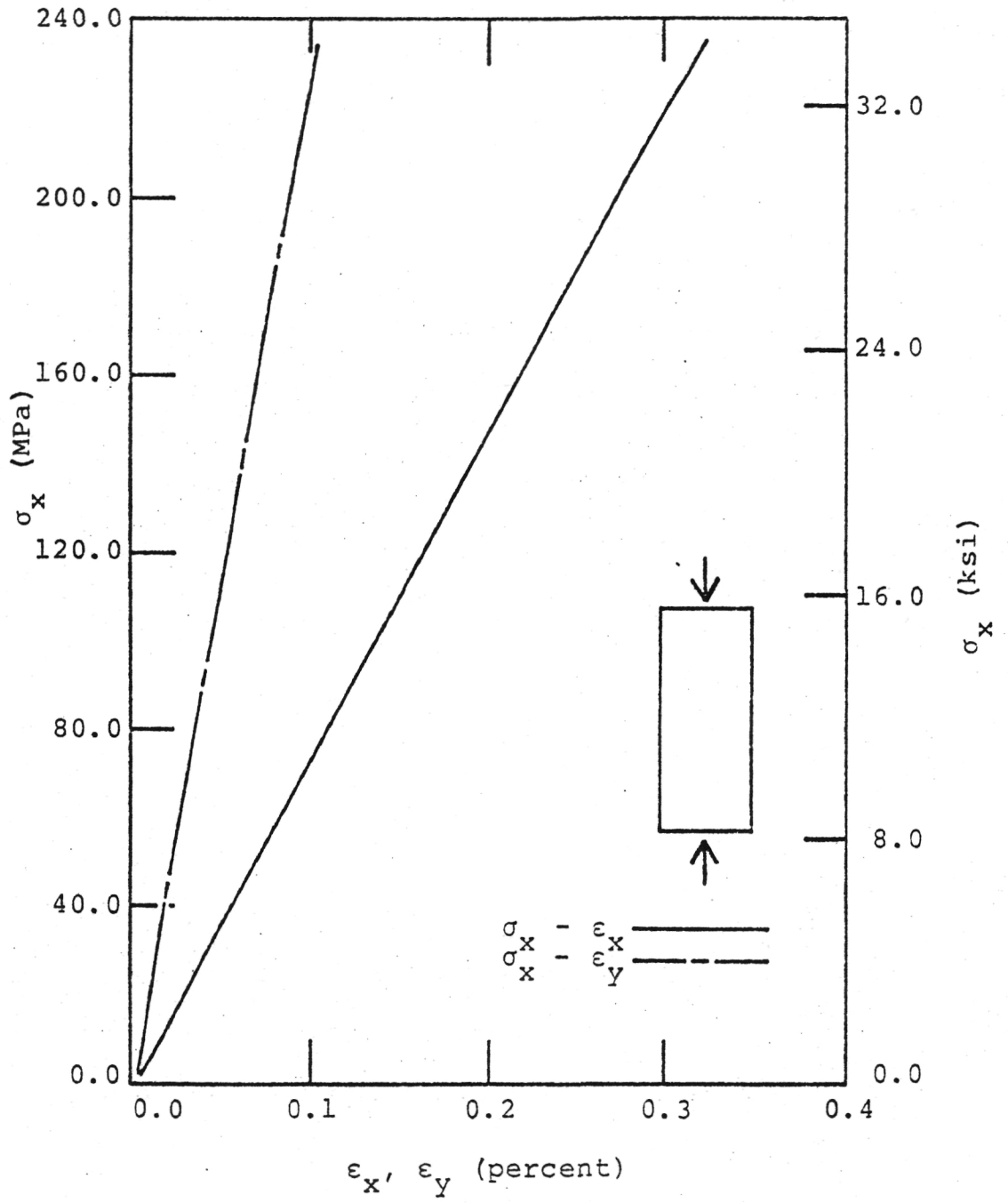

Figure 34. Room Temperature Compressive Stress-Strain Behavior for 2024-T3 Aluminum.

5.3 Comparison of Graphite/Polyimide Tensile and Compressive Data

Table 9 presents average ultimate stress and ultimate strain data. In general the average compressive stresses are significantly larger than the corresponding tensile stresses; in all cases the ultimate compressive strains are larger than the ultimate tensile strains. The only exception is the ultimate compressive stress for a $[0_8]$ laminate which is within the experimental scatter associated with the ultimate tensile stress. However, all $[0_8]$ compressive beams failed at the point of load application, and the ultimate compressive stresses are due to the stress concentrations associated with the loading. Any similar influence from loading is not observed in the other laminate orientations since they fail at much lower stress levels. In general compressive ultimate stresses and ultimate strains for composites are expected to be higher than the respective tensile values.

Any effects on compressive mechanical behavior from the specimen geometry should be noticeable in the elastic data. An initial assumption in the finite element analysis was that the graphite/polyimide system had nearly identical elastic behavior in tension and compression. This characteristic has been observed for metal matrix composites [39]. If the sandwich beam in four-point bending affects the compressive elastic data, these data will exhibit a consistent difference when compared to the corresponding tensile values. For example, the measured compressive Poisson's ratio of the composite may be a function of the mismatch between Poisson's ratio of the honeycomb core and Poisson's ratio of the composite. The honeycomb core has a higher

TABLE 9. COMPARISONS OF ROOM TEMPERATURE TENSILE AND COMPRESSIVE ULTIMATE STRESSES AND STRAINS

Laminate Configuration	Ultimate Stress, σ_x^u			Ultimate Strain, ε_x^u		
	Tension (coupons), MPa (ksi)	Compression (Sandwich beam), MPa (ksi)	Percent difference*	Tension (coupon), %	Compression, (Sandwich beam), %	Percent difference*
$[0_8]$	1354.1 (196.4)	1299.0 (188.4)	-4.1	1.04	1.23	+18.3
$[90_8]$	33.41 (4.86)	213.5 (30.47)	+537	0.42	2.24	+433.3
$[(\pm 45)_2]_s$	109.4 (15.86)	153.5 (22.27)	+40.4	1.22	2.20	+80.3
$[0/\pm 45/90]_s$	450.6 (65.36)	539.2 (78.20)	+19.6	0.98	1.42	+44.9

*Difference from tensile property

Poisson's ratio than all the laminates considered. Since the transverse displacement must be continuous across the composite-honeycomb interface, transverse σ_y stresses are developed. The effect of these stresses on the measured axial strain is shown in Equ. (3.17). This example illustrates possible consistent differences between sandwich beam compressive data and coupon tensile data. These differences may not be as pronounced for some laminate orientations but, nevertheless, are present.

Comparisons of tensile and compressive average Young's modulus, Poisson's ratio, and shear modulus values are shown in Table 10. Significant differences are observed between some tensile and compressive values. However, no consistent trend characterizes these differences. The difference from tensile values to compressive values ranges from a 26.8 percent increase to a 14.2 percent decrease. These differences appear to result from actual material behavior rather than influence of specimen geometry. An examination of graphite/epoxy test results also reveals differences in tensile and compressive properties obtained from similar test specimens [40]. Hence, no effect from the specimen geometry is apparent in the graphite/polyimide elastic properties. The assumption of nearly equal tensile and compressive elastic properties may not be valid for resin matrix material systems.

TABLE 10. COMPARISONS OF AVERAGE ROOM TEMPERATURE TENSILE AND COMPRESSIVE ELASTIC PROPERTIES

Laminate Configuration	Young's Modulus, E_x			Poisson's Ratio, ν_{xy}		
	Tension (coupons), GPa (Msi)	Compression (Sandwich beam), GPa (Msi)	Percent difference*	Tension (coupon)	Compression (Sandwich beam)	Percent difference*
$[0_8]$	131.00 (19.00)	120.45 (17.47)	-8.1	0.331	0.375	+13.3
$[90_8]$	8.27 (1.20)	10.48 (1.52)	+26.7	0.012	0.015	+25.0
$[(\pm 45)_2]_s$	14.55 (2.11)	16.48 (2.39)	+13.3	0.757	0.768	+1.5
$[0/\pm 45/90]_s$	47.78 (6.93)	47.44 (6.88)	-0.7	0.331	0.284	-14.2

	Tension (coupon), GPa (Msi)	Compression, (Sandwich beam), GPa (Msi)	Percent difference*
Shear Modulus, G_{12}	4.19 (0.608)	5.32 (0.771)	+26.8

*Difference from tensile property

Chapter 6

ANALYTICAL RESULTS

6.1 Laminate Analysis

Laminate theory was used to predict Young's modulus and Poisson's ratio for the $[(\pm 45)_2]_s$ and $[0/\pm 45/90]_s$ laminates. A computer program was written to perform the calculations. The program input required the material properties E_1, ν_{12}, E_2, ν_{21} and G_{12} in the natural coordinate system at the test temperature. These properties were determined from tests on $[0_8]$, $[90_8]$, and $[(\pm 45)_2]_s$ laminates, and are shown in Tables 2 through 7.

Table 11 presents comparisons between theory and experiment for tensile properties at room temperature, -157°C (-250°F), and 316°C (600°F). Table 12 presents similar comparisons for compressive properties at room temperature. All predicted Young's modulus values and most of the predicted Poisson's ratio values are larger than the corresponding experimental properties. More than three-fourths of the calculated properties differed from average experimental values by less than ten percent. As seen in the tables, the maximum difference for the remaining properties was approximately twenty percent. No trend was apparent for these larger differences. To be acceptable for engineering predictions of actual laminate response it is desirable that all calculated values be within ten percent of the experimental values. Hence, laminate theory predicted approximate elastic properties, but in some cases, did not obtain the required accuracy to be used as a high level design tool. Further investigation of the discrepancies between

TABLE 11. COMPARISON OF EXPERIMENTAL AND PREDICTED ELASTIC TENSILE DATA

Laminate Configuration	Test temperature, °C (°F)	Young's Modulus, E_x			Poisson's Ratio, ν_{xy}		
		Experimental, GPa (Msi)	Laminate theory, GPa (Msi)	Percent difference*	Experimental	Laminate theory	Percent difference*
$[(\pm 45)_2]_s$	RT+	14.55 (2.11)	15.03 (2.18)	+3.3	0.757	0.790	+4.4
	-157 (-250)	17.79 (2.58)	18.13 (2.63)	+1.9	0.682	0.763	+11.9
	316 (600)	8.69 (1.26)	9.44 (1.37)	+8.7	0.718	0.865	+20.5
$[0/\pm 45/90]_s$	RT+	47.78 (6.93)	49.92 (7.24)	+4.5	0.331	0.302	-8.8
	-157 (-250)	44.13 (6.40)	48.88 (7.09)	+10.8	0.314	0.360	+14.6
	316 (600)	45.16 (6.55)	47.92 (6.95)	+6.1	0.340	0.315	-7.4

*Difference from experimental value
+Room temperature

TABLE 12. COMPARISON OF ROOM TEMPERATURE EXPERIMENTAL AND PREDICTED ELASTIC COMPRESSIVE DATA

Laminate Configuration	Young's Modulus, E_x			Poisson's Ratio, ν_{xy}		
	Experimental, GPa (Msi)	Laminate theory, GPa (Msi)	Percent difference*	Experimental	Laminate theory	Percent difference*
$[(\pm 45)_2]_s$	16.48 (2.39)	18.34 (2.66)	+11.3	0.768	0.728	-5.2
$[0/\pm 45/90]_s$	47.44 (6.88)	48.12 (6.98)	+1.5	0.284	0.289	+1.8

*Difference from experimental value

laminate theory and experiment was not undertaken as that was not the main goal of this study.

6.2 Finite Element Analysis

The finite element method was used to perform a stress analysis on a portion of the sandwich beam test section (Figure 6). Graphite/polyimide and boron/aluminum flanges with $[0_8]$, $[90_8]$, $[(\pm 45)_2]_s$, and $[0/\pm 45/90]_s$ orientations were investigated at room temperature. A sandwich beam with 2024-T3 aluminum flanges was also studied. Input properties for the finite element computer program were obtained from either experiment, the literature [34,39,41,42] or laminate theory. Graphite/polyimide values were unavailable, for ν_{23}, and graphite/epoxy data were substituted [43]. A summary of all composite and honeycomb input properties for the finite element analysis are available in the Appendix. Equilibrium checks were included in the finite element program to compare the resultants of the reaction forces with the applied load resultants. All predicted values satisfied equilibrium.

The transverse stress in the top flange, $\bar{\sigma}_y$, and the "interlaminar" shear stress between the top flange and honeycomb core, $\bar{\tau}_{yz}$, were the most important calculated values. These stresses can be related through an equilibrium equation. As shown in Equ. (3.17), $\bar{\sigma}_y$ can influence the axial midplane strain of a composite laminate through the Poisson effect. Specifically, the effect of $\bar{\sigma}_y$ on observed strain data depends upon the magnitude of $\bar{\nu}_{xy}\bar{\sigma}_y/\bar{\sigma}_x$. If,

$$\bar{\nu}_{xy} \frac{\bar{\sigma}_y}{\bar{\sigma}_x} \simeq 0 \tag{6.1}$$

then Equ. (3.17) reduces to

$$\varepsilon_x^o = \frac{\bar{\sigma}_x}{\bar{E}_x} \tag{6.2}$$

A form of Equ. (6.2) has been used to calculate Young's modulus for the top flange of the sandwich beam, i.e.

$$\bar{E}_x = \frac{\bar{\sigma}_x}{\varepsilon_x^o} \tag{6.3}$$

where the measured axial strain is assumed to be constant through the flange thickness. However, if Equ. (6.1) is not true for sandwich beam specimens, a biaxial stress state exists in the top flange, and previous calculations of Young's modulus using Equ. (6.3) would not be accurate.

The results from the finite element analysis are shown in Table 13. In each case the calculated $\bar{\sigma}_x$ was nearly constant in the top flange as expected. Calculations for $\bar{\tau}_{yz}/\bar{\sigma}_x$ are not shown in the table since these values were less than 0.001 in all cases. Hence, $\bar{\tau}_{yz}$ is negligible. Calculations for $(-\bar{\nu}_{xy}\bar{\sigma}_y/\bar{\sigma}_x)$ are shown for graphite/ polyimide, boron/aluminum, and 2024-T3 aluminum top flanges. All values are less than 0.01 with the isotropic aluminum flange having the largest value and the graphite/polyimide flanges exhibiting the smallest values. The calculations use the average linear elastic Poisson's ratio for each top flange of the beam. If an instantaneous Poisson's ratio was an order of magnitude larger than the linear elastic value, the calcu-

TABLE 13. FINITE ELEMENT RESULTS FOR BIAXIAL STRESS EFFECTS IN TOP FLANGE OF SANDWICH BEAM

Top flange of beam	Material system	$-\bar{\nu}_{xy} \frac{\bar{\sigma}_y}{\bar{\sigma}_x}$
$[0_8]$	graphite/polyimide	0.0001
	boron/aluminum	0.0033
$[90_8]$	graphite/polyimide	0.0001
	boron/aluminum	0.0038
$[(\pm 45)_2]_s$	graphite/polyimide	0.0005
	boron/aluminum	0.0066
$[0/\pm 45/90]_s$	graphite/polyimide	0.0001
	boron/aluminum	0.0061
2024-T3	aluminum	0.0099

lations would still indicate an effect which is less than the approximate ten percent experimental scatter. Hence, the analysis predicts the test section of the top flange to be in an essentially uniform, uniaxial compressive stress state and indicates that the influence of the small biaxial stresses on the measured material response is negligible. The analysis does indicate that the influence of biaxial stresses is larger for metal matrix composites than for resin matrix composites; nevertheless, this influence is still negligible.

Chapter 7

SUMMARY AND CONCLUSIONS

The results of a comprehensive experimental and analytical study of the sandwich beam as a compressive test method for composite laminates have been presented. An integral phase of the experimental portion of the study was the development of tensile and compressive material properties for HTS/PMR-15 graphite/polyimide laminates. The tensile properties were obtained at room temperature, -157°C (-250°F), and 316°C (600°F); compressive properties were obtained at room temperature only. The effects of temperature on the tensile elastic properties were presented, and the tensile and compressive room temperature properties were compared. Also included in the experimental program were results for some compressive elastic properties of 2024-T3 aluminum alloy and 5052 aluminum honeycomb. The observed properties for 2024-T3 aluminum were compared with documented results. The compressive honeycomb data and the tensile composite data were required for input into a three-dimensional finite element analysis of the sandwich beam. In addition to this finite element analysis, the analytical portion of this study included comparisons of average experimental elastic properties for composite laminates with the corresponding predicted properties from lamination theory.

The major conclusions from the experimental and analytical results follow:

1. The sandwich beam in four-point bending can be used

to obtain accurate, reliable compressive Young's modulus and Poisson's ratio data for composite laminates. This conclusion is based upon (a) no apparent effects from specimen geometry on elastic properties, (b) an essentially uniform, uniaxial compressive stress state prediction from the finite element analysis, and (c) accurate Young's modulus and Poisson's ratio values for 2024-T3 aluminum using the sandwich beam specimen.

2. Ultimate compressive stresses obtained from sandwich beam specimens should be evaluated for dependence on local stress concentrations. Although the $[90_8]$, $[(\pm 45)_2]_s$, and $[0/\pm 45/90]_s$ beam specimens failed in the test section, the $[0_8]$ beams failed at the point of load application. The ultimate compressive stress for the $[0_8]$ laminate is dependent on stress concentrations due to loading.
3. Ultimate stresses at -157°C and 316°C were as much as thirty-two percent lower than the corresponding room temperature value. The $[0_8]$ and $[0/\pm 45/90]_s$ laminates were affected most significantly at the low temperature, and the $[(\pm 45)_2]_s$ and $[90_8]$ laminates were affected most significantly at the elevated temperature.
4. Strength degradation at lower temperatures is believed to be associated with the increase in thermal stresses and resulting material damage.

5. Significant temperature dependence of Young's modulus was evident only in the $[90_8]$ and $[(\pm 45)_2]_s$ laminates. The modulus of these laminates increased with decreasing temperature.
6. Young's modulus and Poisson's ratio for HTS/PMR-15 laminates in this study were not the same in tension and compression. Differences ranged from a 26.7 percent increase to a 14.2 percent decrease from the tensile values. No consistent trend characterized these differences.
7. Lamination theory can predict Young's modulus and Poisson's ratio for HTS/PMR-15 laminates but in some cases, lacks sufficient accuracy to be a high level design tool. The maximum difference between theory and experiment was approximately twenty percent.

BIBLIOGRAPHY

1. Standard Method of Test for Compressive Properties of Rigid Plastics, D695-69, 1975 Annual Book of ASTM Standards, Part 35, American Society for Testing and Materials, 1975.

2. Hoggatt, J. T., "Test Methods for High-Modulus Carbon Yarn and Composites," Composite Materials: Testing and Design, ASTM STP 460, American Society for Testing and Materials, 1969, pp. 48-61.

3. Adsit, N. R., and Forest, J. D., "Compression Testing of Aluminum-Boron Composites," Composite Materials: Testing and Design, ASTM STP 460, American Society for Testing and Materials, 1969, pp. 108-121.

4. Elkin, R. A., Fust, G., and Hanley, D. P., "Characterization of Graphite Fiber/Resin Matrix Composites," Composite Materials: Testing and Design, ASTM STP 460, American Society for Testing and Materials, 1969, pp. 321-335.

5. Plastics for Aerospace Vehicles, Part 1, Reinforced Plastics, Military Handbook, MIL-HDBK-17A, Department of Defense, 1971. (Primary sources - reference 1 and Dastin, S. J., Lubin, G., Munyak, J. A., Rosenberg, M., and Slobodzinski, A., "Determination of Principal Properties of "E" Fiberglass High Temperature Epoxy Laminates for Aircraft." DAAA21-68-C-0404, Grumman Aircraft Engineering Corporation, August 1969.)

6. Ewins, P. D., "Tensile and Compressive Test Specimens for Unidirectional Carbon Fibre Reinforced Plastics," Technical Report 71217, Royal Aircraft Establishment, 1971.

7. Purslow, D., and Collings, T. A., "A Test Specimen for the Compressive Strength and Modulus of Unidirectional Carbon Fibre Reinforced Plastic Laminates." Technical Report 72096, Royal Aircraft Establishment, 1972.

8. Bert, Charles, W., "Experimental Characterization of Composites," Composite Materials, Volume 8, Part 2, Academic Press, Inc., 1975.

9. Kulkarni, S. V., Rice, J. S., and Rosen, B. W., "An Investigation of Kevlar 49/Epoxy Composites," Composites, Volume 6, September 1975, pp. 217-225.

10. Walker, A. R. and Williams, D. N., "Experimental Determination of Mechanical Properties of Unidirectional Carbon Fibre Reinforced Plastics in Compression," B. S. Thesis, Bristol University (England), 1976.

11. Waddoups, M. E., "Characterization and Design of Composite Materials," Composite Materials Workshop, S. W. Tsai, J. C. Halpin, and N. J. Pagano, eds., Technomic Publishing Co., Inc., 1968, pp. 254-308.

12. Dastin, S., Lubin, G., Munyak, J., and Slobodzinski, A., "Mechanical Properties and Test Techniques for Reinforced Plastic Laminates," Composite Materials: Testing and Design, ASTM STP 460, American Society for Testing and Materials, 1969, pp. 13-26.

13. Hadcock, R. N., and Whiteside, J. B., "Special Problems Associated with Boron/Epoxy Test Specimens," Composite Materials: Testing and Design, ASTM STP 460, American Society for Testing and Materials, 1969, pp. 27-36.

14. Lenoe, E. M., Knight, M., and Schoene, C., "Preliminary Evaluation of Test Standards for Boron/Epoxy Laminates," Composite Materials: Testing and Design, ASTM STP 460, American Society for Testing and Materials, 1969, 122-139.

15. Grimes, G. C., Francis, P. H., Commerford, G. E., Wolfe, G. K., "An Experimental Investigation of the Stress Levels at which Significant Damage Occurs in Graphite Fiber Plastic Composites," AFML-TR-72-40, May 1972.

16. Hofer, Kenneth E., Rao, P. N., Humphreys, V. E., "Development of Engineering Data on the Mechanical and Physical Properties of Advanced Composites Materials," Technical Report AFML-TR-72-205-Part I, IIT Research Institute, 1972.

17. "Standard Method of Test for Compressive Properties of Oriented Fiber Composites," D3410-75, 1975 Annual Book of ASTM Standards, Part 36, American Society for Testing and Materials, 1975.

18. Ho, T., "A Compressive Test Method for Composites," Materials Review '75: Proceedings of the Seventh National Technical Conference (SAMPE), October 1975, pp. 295-297.

19. Godfried, L. M., "Compressive Test Method for Fibre Reinforced Composites," Report No. FOR-R-1877, Royal Netherlands Aircraft Factories Fokker, 1975.

20. Ryder, J. T., and Black, E. D., "Compression Testing of Large Gage Length Composite Coupons," Composite Materials: Testing and Design (Fourth Conference), ASTM STP 617, American Society for Testing and Materials, 1977, pp. 170-189.

21. Davis, John G., Jr., "Compressive Strength of Lamina Reinforced and Fiber Reinforced Composite Materials," Ph.D. Dissertation, VPI&SU, May 1973.

22. Knoell, A. C., "Evaluation of Boron/Aluminum Tubes in Compression," AIAA Paper No. 75-789, AIAA/ASME/SAE 16th Structures, Structural Dynamics and Materials Conference, May 1975.

23. Kreider, K. G., "Mechanical Testing of Metal Matrix Composites," Composite Materials: Testing and Design, ASTM STP 460, American Society for Testing and Materials, 1969, pp. 203-214.

24. Weidner, John C., "New Tensile and Compressive Test Specimens for Unidirectionally Reinforced Graphite Epoxy Composites," Technical Report AFML-TR-70-264, University of Dayton Research Institute, 1971.

25. Baldwin, D. H., Sierakowski, R. L., "Fracture Characteristics of a Metal Matrix Composite-Aluminum Alloy Matrix-Stainless Steel Fibers," Composites, Volume 6, January 1975, pp. 30-34.

26. "Standard Method of Test for Edgewise Compressive Strength of Flat Sandwich Constructions," C364-61 (Reapproved 1970). 1975 Annual Book of ASTM Standards, Part 25, American Society for Testing and Materials, 1975.

27. Suarez, J. A., Whiteside, J. B., and Hadcock, R. N., " The Influence of Local Failure Modes on the Compressive Strength of Boron/Epoxy Laminates," Composite Materials: Testing and Design (Second Conference) ASTM STP 497, American Society for Testing and Materials, 1972, pp. 237-256.

28. Advanced Composite Airframe Structures, First Monthly Progress Report for AF Contract F 33615-68-C-1301, Grumman Aircraft Corporation, March 1967.

29. Herakovich, C. T., Davis, Jr., J. G., and Viswanathan, C. N., "Tensile and Compressive Behavior of Borsic/Aluminum," Composite Materials: Testing and Design, (Fourth Conference) ASTM STP 617 American Society for Testing and Materials, 1977, pp. 344-357.

30. Ashton, J. E., Halpin, J. C., Petit, P. H., Primer on Composite Materials: Analysis, Technomic Publishing Co., Inc., 1969.

31. Ashton, J. E., and Whitney, J. M., Theory of Laminated Plates, Technomic Publishing Co., Inc., 1970.

32. Jones, Robert M., Mechanics of Composite Materials, Scripta Book Company, 1975.

33. Popov, E. P., Mechanics of Materials, Prentice-Hall, Inc., 1952.

34. Metals Handbook, Taylor Lyman, ed., 8th edition, vol. 1, American Society for Metals, 1961.

35. Herakovich, Carl T., and Brooks, Ernest W. Jr., "Tensile Strength Behavior of Composite Reinforced Metals," VPI-E-73-5, VPI&SU, January 1973.

36. Askins, D. Robert, "Development of Engineering Data on Advanced Composite Materials," AFML-TR-77-151, University of Dayton Research Institute, September 1977.

37. Rosen, B. Walter, "A Simple Procedure for Experimental Determination of the Longitudinal Shear Modulus of Unidirectional Composites," Journal of Composite Materials, vol. 6, October 1972, pp. 552-554.

38. Shuart, Mark J. and Herakovich, Carl T., "Tensile and Compressive Test Results for Metal Matrix Composites," VPI-E-77-6, VPI&SU, February 1977.

39. Kennedy, John M., Tenney, Darrel R., and Herakovich, Carl T., "Tensile and Compressive Stress-Strain Behavior of Heat Treated Boron-Aluminum," presented at the Second International Conference on Composite Materials, Toronto, Canada, April 1978.

40. Flight-Service Program for Advanced Composite Rudders on Transport Aircraft, Fifth Quarterly Report for Contract NAS1-12954, Douglas Aircraft Company, May 1975.

41. Bush, Harold G. and Welker, Tanchum, "A Biaxial Method for Inplane Shear Testing," NASA TM 74070, 1978.

42. Herakovich, C. T., Renieri, G. D., and Brinson, H. F., "Finite Element Analysis of Mechanical and Thermal Edge Effects in Composite Laminates," Composite Materials: The Influence of Mechanics of Failure on Design, Army Symposium on Solid Mechanics, Cape Cod, MA, September 1976.

43. Kriz, Ronald D., "Effect of Material Properties on Interlaminar Stresses in Angle-Ply Composite Laminates," VPI-E-77-16, VPI&SU, March 1977.

APPENDIX

MATERIAL PROPERTY INPUT FOR FINITE ELEMENT ANALYSIS

The composite and honeycomb material properties for the finite element analysis are shown in Table A-1. These properties were obtained from either experiment, the literature [34,39,41-43], or laminate theory. The Poisson's ratio values for the honeycomb, ν_{TL} and ν_{TW}, were calculated from the basic equations of strength of materials. Assuming the angles of each hexagonal cell are rigid, it can be shown,

$$\nu_{TL} = \nu_{TW} = \nu_{Al} \tag{A.1}$$

where ν_{Al} is the Poisson's ratio of 5052 aluminum alloy.

A two-dimensional finite element analysis of the honeycomb core cell structure also was performed to predict E_L and ν_{LW}. This analysis used rod elements to approximate the structure and assumed the rods to be rigidly connected. A comparison of average experimental values and predicted values is presented in Table A-2. Although the calculated Poisson's ratio is more than seventeen percent lower than the experimental value, the correlation between theory and experiment is sufficiently close to have confidence in the experimental results.

TABLE A-1. MATERIAL INPUT PROPERTIES FOR THE 3-D FINITE ELEMENT ANALYSIS

Material description	E_x, GPa (Msi)	G_{xy}, GPa (Msi)	ν_{xy}	E_y, GPa (Msi)	G_{yz}, GPa (Msi)	ν_{yz}	E_z, GPa (Msi)	G_{zx}, GPa (Msi)	ν_{zx}
Gr/PI, $[0_8]$	131.0 (19.0)	4.20 (0.607)	0.331	8.27 (1.20)	3.41 (0.494)	0.501	8.27 (1.20)	4.20 (0.607)	0.021
Gr/PI, $[90_8]$	8.27 (1.20)	4.20 (0.607)	0.021	131.0 (19.0)	4.20 (0.607)	0.331	8.27 (1.20)	3.41 (0.494)	0.501
Gr/PI, $[(\pm45)_2]_s$	14.55 (2.11)	33.72 (4.89)	0.757	14.55 (2.11)	3.79 (0.550)	0.104	10.48 (1.52)	3.79 (0.550)	0.075
Gr/PI, $[0/\pm45/90]_s$	47.78 (6.93)	18.89 (2.74)	0.331	47.78 (6.93)	3.79 (0.550)	0.346	10.48 (1.52)	3.79 (0.550)	0.076
B/Al $[0_6]$	217.0 (31.47)	46.88 (6.8)	0.332	148.0 (21.46)	25.92 (3.76)	0.33	68.95 (10.0)	46.88 (6.8)	0.106
B/Al $[90_8]$	148.0 (21.46)	46.88 (6.8)	0.226	217.0 (31.47)	46.88 (6.8)	0.332	68.95 (10.0)	25.92 (3.76)	0.154
B/Al $[(\pm45)_2]_s$	125.0 (18.13)	57.71 (8.37)	0.411	125.0 (18.13)	29.10 (4.22)	0.249	55.30 (8.02)	29.10 (4.22)	0.110
B/Al $[0/\pm45/90]_s$	128.9 (18.7)	47.57 (6.90)	0.356	128.9 (18.7)	29.10 (4.22)	0.295	55.30 (8.02)	29.10 (4.22)	0.126
5052 aluminum honeycomb*	0.00177 (0.000256)	0.221 (0.032)	1.10	(0.00104) (0.000151)	(0.283) (0.041)	0.000207	1.65 (0.240)	0.676 (0.098)	0.33

*(x,y,z) correspond to (L,W,T), respectively

TABLE A-2. COMPARISON OF PREDICTED AND EXPERIMENTAL ROOM TEMPERATURE ELASTIC PROPERTIES FOR 5052 ALUMINUM HONEYCOMB

Material Property	Experimental results	Finite Element results	Percent difference*
E_L, kPa (psi)	1765.0 (256.0)	1909.8 (277.0)	+8.2
ν_{LW}	1.10	0.9111	-17.2

*Difference from experimental value

1. Report No.	2. Government Accession No.	3. Recipient's Catalog No.
NASA TM-78783		

4. Title and Subtitle	5. Report Date
AN EVALUATION OF THE SANDWICH BEAM IN FOUR-POINT BENDING AS A COMPRESSIVE TEST METHOD FOR COMPOSITES	SEPTEMBER 1978
	6. Performing Organization Code

7. Author(s)	8. Performing Organization Report No.
MARK J. SHUART, CARL T. HERAKOVICH*	
	10. Work Unit No. 524-71-03-01

9. Performing Organization Name and Address	11. Contract or Grant No.
NASA LANGLEY RESEARCH CENTER HAMPTON, VIRGINIA 23665	
	13. Type of Report and Period Covered
12. Sponsoring Agency Name and Address	TECHNICAL MEMORANDUM
NATIONAL AERONAUTICS AND SPACE ADMINISTRATION WASHINGTON, DC 20546	14. Sponsoring Agency Code

15. Supplementary Notes

*VIRGINIA POLYTECHNIC INSTITUTE AND STATE UNIVERSITY
BLACKSBURG, VIRGINIA 24061

16. Abstract

Results of analytical and experimental studies on the honeycomb sandwich beam in four-point bending are presented. The experimental phase of the study includes compressive tests on HTS/PMR-15 graphite/polyimide, 2024-T3 aluminum alloy, and 5052 aluminum honeycomb at room temperature, and tensile tests on graphite/polyimide at room temperature, -157°C (-250°F), and 316°C (600°F). Elastic properties and strength data are presented for $[0_8]$, $[90_8]$, $[(\pm 45)_2]_S$, and $[0/\pm 45/90]_S$ laminates.

The room temperature elastic properties were generally found to differ in tension and compression with Young's modulus values differing by as much as twenty-six percent. The effect of temperature on modulus and strength was shown to be laminate dependent. A three-dimensional finite element analysis predicted an essentially uniform, uniaxial compressive stress state in the top flange test section of the sandwich beam.

In conclusion, the sandwich beam can be used to obtain accurate, reliable Young's modulus and Poisson's ratio data for advanced composites; however, the ultimate compressive stress for some laminates may be influenced by the specimen geometry.

17. Key Words (Suggested by Author(s))	18. Distribution Statement
COMPRESSION SANDWICH BEAM TEST METHODS TENSION COUPONS ELEVATED TEMPERATURE FINITE ELEMENT	UNCLASSIFIED-UNLIMITED SUBJECT CATEGORY 71

19. Security Classif. (of this report)	20. Security Classif. (of this page)	21. No. of Pages	22. Price*
UNCLASSIFIED	UNCLASSIFIED	105	$6.50

* For sale by the National Technical Information Service, Springfield, Virginia 22161